Response to the reviewer #1

Formatted: Heading 2

#	Comments from Referees #1	Author's response	Author's changes in manuscript
1	In data processing, when you work on amplitude and phase of the signal, the frequency response of both seismic and infrasonic sensors is a crucial point. This is especially true in this work, where frequency range of signals that you are analysing, is at the bound of the linear frequency response of some of the used sensors. As you show in Figures 3 and 6, you hold the frequency response curve of Microbarometers MB2000, and GS-21 and CMG-3V seismic sensors, I was wondering, did you correct the signal for the frequency response?	As the sensors used in infrasound investigations are broadband the correction for the frequency response is not applied applied when prior PMCC processing. For the data of the ABKAR, KKAR, and MKAR, it is assumed that the frequency response of all sensors of a same array are identical. As PMCC is a correlation based method, identical phase shift should not affect the detection. However, to get reliable amplitude measurements, should be corrected for the instrumental response. For the purpose of this study, , this is not a critical point as the phase responses of the CMG-21 are stable and the absence of the correction doesn't affect the accuracy of the azimuth determination using PMCC. Surely the absolute amplitudes are measured with a large error. However, the absolute amplitude determination is not essential, only relative amplitudes are compared with modeling results.	
2	I order to make the overall structure of the paper clearer, I believe that few paragraphs of the introduction section could be moved into the method section (for example lines 34-36 and lines 69-76), or in the discussion section (e.g. lines 36-40). I think this would	Accepted	Lines 34-36 and lines 69-76 are moved to the methods section. Lines 36-40 are moved to the discussion section.

	also help to streamline the introduction section.		
3	you could better highlight: i) the contribution of this paper to the literature and ii) the goal of your study and how you try to reach it. You mention that you analysed a long-time interval with simultaneous seismic and infrasonic recording, but it is not so clear if this kind of study, using dense network and lots of data, has been already done in literature.	To our knowledge, multi-year ambient noise comparisons between co-located seismic and infrasound sensors have not been performed before.	One sentence has been added in the introduction.
4	I suggest that you try to use Rose Diagrams, they could help you representing better the results (both azimuth and frequency of each class) of Figures 13 and 14.	Accepted	Figures 13 and 14 are reshaped as the rose diagrams (the new numbers are 15 and 16).
5	I suggest an English revision, in order to make the manuscript reading more fluent.	Accepted	The English has carefully been revised
6	The bibliography is not cited uniformly throughout the manuscript	Accepted	TODO Citations has carefully been checked throughout the paper
7	Figure 3: x labels are wrong	Accepted	Figure 3 is reconstructed altogether with the labels.
8	Figure 7, 8 and 9: Can you put the legend out of the plot? They overwrite the results.	Accepted	The legends are moved out (new numbers are 8, 9 and 10).
9	Insert in all the different plot of figures 13 and 14 the letters (e.g. a, b etc).	Accepted	The letters are inserted (new numbers are 15 and 16).
10	Line 49-50: Specify which kind of algorithm do you refer to.	Accepted	This has been clarified
11	Line 53: were	Accepted	
12	Line 58: measured instead of “measuring”	Accepted	
13	Line 64-65: “These agreements have been improved using more accurate wind profiles obtained from high resolution LIDAR middle atmospheric sounding”. It is not clear that this work has been done by Hupe et al 2018.	Accepted	The reference to the Hupe et al 2018 is inserted.
14	Line 66-67: “In this paper, we further extend the approach developed by Hupe at al. (2018) using microbarom recorded by the dense Kazakhstani network”. Specify in which sense you extended the work, only in terms of number of station/network?	Accepted	This has been clarified
15	Line 70: rephrase “For microseisms, the bathymetry strongly affects the source intensity”	Accepted	The bathymetry strongly affects the source intensity in microseism modelling

	in "The bathymetry strongly affects the source intensity in microseism modelling"		
16	Line 72: "angles lower than 40" instead of "angles lower the 40"	Accepted	
17	Line 74: typing error	Corrected	
18	Line 83: "as it contains a five seismic and three infrasound arrays". In the abstract and later on into the text and figure 1 you say four seismic arrays.	The BVAR was not shown at Figure1. There are 5 arrays now.	
19	Line 89: "MKIAR (9 elements), and in Makanchi village" is not clear, MKIAR is in Makanchi village?	Corrected	The infrasound network consists of the IMS infrasound station IS31 located in north-west Kazakhstan (2.1 km aperture, 8 elements), two national arrays of 1 km aperture: KURIS (4 elements) near the Kurchatov, MKIAR (9 elements) near the Makanchi village
20	Line 83: "as it contains a five seismic and three infrasound arrays". In the abstract and later on into the text and figure 1 you say four seismic arrays.	Corrected	Five seismic
21	Line 92: cut Figure 3	Corrected	It is Figure 1 now.
22	Line 101: cut Figure 5	Corrected	It is Figure 1 now.
23	Line 120-121: Add references		
24	Line 132-134: Understanding this point is difficult in this part of the text, maybe you could move it into the results or discussion section, where you can refer to the figures. Or add here that it would be clarified later into the text.	Accepted and deleted as the same is stated again in the discussion section.	
25	Line 147-151: Specify that you are describing Fig. 7	Accepted	The reference to Picture 8 is added
26	Line 155: "amplitude increases from 0.001 to 0.03 Pa" are those average values?	No, these are the maximal values.	the maximal signal amplitude increases from 0.001 to 0.03 Pa.
27	Line 156: I suspect that "repeatable" means replicable.	No, actually it is the repetitive.	"with repetitive seasonal variations"
28	Line 171: "a decrease in amplitude is observed early January 2017 at all stations." It is difficult to see this decreasing trend.	The amplitude scales are uniform now. The effect must be more visible.	
29	Line 182-183: "As the used source model was developed for microseisms (Ardhuin et al., 2011), an empirical scaling factor (F = 1:10000) must be applied for comparing the observed to the predicted amplitudes". Could you give further details?	Accepted	This has been clarified

30	Line 187-190. Could you explain better the reason of the discrepancy? And comment the quantitative estimations of the prediction quality?	Accepted	This has been clarified
31	Line 192-194: I think it is important here to highlight the further data you analyse in your work, both in terms of time interval and number of stations.	Accepted	This has been mentioned in the discussion
32	Line 200: Do you mean the comparison between observations and simulations?	No, we mean but not the comparison but both of them do.	Observations as well as simulations, show large temporal variations in the dominating microbarom source regions explained by the seasonal reversals of the prevailing stratospheric winds, which in turn, cause the migration of storm activity area to the winter hemisphere (Stutzmann et al., 2012).
33	Line 200-202: I suggest that you explain better this point.	Accepted	This has been clarified
34	Line 208: "Simulating microbaroms predicts signals" maybe Simulated microbaroms predict signals.	Accepted	
35	Line 208-210: Refer to the figures	The reference is added	"observed only at IS31 and MKAR, Figure 15 c."
36	Line 222: Could you specify here the expanded form of SSW (beside the abstract)?	Accepted	
37	Line 222-227: As you write here, this topic seems to be one of the findings of the paper.	Yes, as stated in the text	
38	Line 243-244: This is not reported elsewhere in the text, maybe you could highlight this aspect even in other section, if you believe that it is an important point of your work.	Accepted	This result is expanded in the discussion.

Formatted: English (United States)

Formatted: Normal

Response to the reviewer #2

Formatted: Heading 2

#	Comments from Referees #2	Author's response	Author's changes in manuscript
1	I missed in the abstract and introduction some discussion on the novelty of this study: e.g. what the added value is of a characterisation with seismic and acoustic arrays that are part of a dense network.	Accepted	To our knowledge, systematic comparisons between observed and predicted microseisms and microbaroms were not carried out. This paper confirms the pioneer findings of Donn by considering several years of observations at a dense regional seismo-acoustic network. Such comparisons confirm a common source mechanism of seismic and acoustic ocean ambient noise while highlighting the influence of long-range atmospheric propagation on microbarom prediction. This has been clarified in the text.
2	In the conclusion, the authors claim that analyzing multiyear archives of continuous recordings yields additional information about the spatial and temporal variability of the ambient noise originating from two hemispheres. This is an interesting aspect, but in my opinion the manuscript does not provide sufficient evidence for that.	Accepted	The issue is excluded from the conclusion
3	A shortcoming is the lack of microseism predictions. Certainly since these simulations can be produced by the same model. Please add these to a revised manuscript.	Accepted	The microseism predictions are inserted. This is done via the addition of Figures 12 – 14. The predictions calculation is described in the method section. The results are discussed in the section results and discussions.
4	I also missed a more direct comparison of microseism and microbarom observations, e.g. MKIAR/MKAR and KURIS/Kurchatov	Accepted	The comparison is done via the placement of figures 19 and 20. The comparison is described in the discussion section.
5	Figures 1, 2, 4 and 5 could be combined in one single figure.	Accepted	The figures are combined into the new version of figure 1.
6	missed figures that: (1) show a map of the distribution and characteristics (amplitude/dominant frequency) of microbarom and microseism sources that are considered in this study (also from the southern hemisphere?)	Accepted	These maps are inserted as figures 6 and 7 for microbarom and microseism sources accordingly. The description is done in the methods section.
7	missed figures that: (2) spectral characteristics of the observations, i.e. Probability Density Functions of the Power Spectral Densities for winter and summer months, for all arrays considered.	Accepted	The PSDs are shown in picture 4. The description is at the observation network section.

8	I would like the authors to address spelling and grammatical errors. I have included a few suggestions and have included a rephrasing occasionally.	Accepted and checked where possible.	
9	I would like the authors to discuss the shortcomings in the current method (data processing, range-independence) in a revised version of the manuscript. In particular, the used array processing method is known to produce biased results when the signal consists of multiple, concurrent sources (the case when studying microbarons).	Accepted	This limitation is now clearly addressed in the conclusion.
10	Line 10 In the asbtract: - describe the results in more detail - what are the differences between modeling and observations? - not much emphasis on the microseism signals - what is the broader perspective of this characterization using seismic and acoustic arrays?	Accepted	The outcomes of this study were reformulated (see point 1).
	Line 14 that are part	Accepted	
11	Line 25 Microseism and microbarom modeling techniques were preceded by years of observations. Add a paragraph on the history observations of microseisms and microbaroms to introduce the topic of this paper; e.g. the work by Benioff and Gutenberg. I also missed a review of the work by Donn and Rind from the 1970s which is important to mention. Rind also published a study in 1980 discussing the joint observation of microseisms and microbaroms.	Accepted	Reviews of pioneer work on microseism microbaroms have been added in the introduction.
12	Line 29 Microbaroms and microseisms are not only generated in the middle of the ocean by opposing wavetrains but also near coastlines (coastal reflection). Discuss this	Accepted	See point 11.
13	Line 29 Introduce primary and secondary microseisms. The primary microseisms do not have a counterpart in the atmosphere. Discuss why.	Accepted	See point 11.

14	Line 29 This study would certainly benefit from a Figure that shows probability density functions of the power spectral density of co-located microbarom and microseism arrays, in particular KURIS/Kurchatov and MKAR/MKIAR	Accepted	The comparison is shown by new figures (19 and 20) and described in the discussion section.
15	Line 31 Explain how the Rayleigh waves are predicted by the acoustic pressure source. Are there also homogenous P-waves generated?	Accepted	One reference is added.
16	Line 32 I would move this paragraph after (KNMI network, Evers and Haak 2001).	Accepted	The paragraph moved to the method section.
17	Line 35 this is a major assumption. Why is the impedance condition not taken into account?	Accepted	We agree. The bathymetry effect plays an important role when calculating the microseism source intensity as resonance effects occur leading to a modulation of the pressure fluctuations at the ocean bottom. This effect has been modeled using compressible amplification factor of Stutzmann et al. (2012). This has been clarified in the manuscript.
18	Line 41 I would move this paragraph after (KNMI network, Evers and Haak 2001).	Accepted	The paragraph is moved to the recommended place.
19	Line 46 needs an introduction how microbaroms relate to microseisms	Accepted	See point 11.
20	Line 49 Include a paragraph to review recent articles on high-resolution beamforming methods for microseisms (Gal et al., 2016) and microbaroms (Ouden et al., 2020). Such methods are absolutely needed to resolve the complex infrasonic wavefield at microseism/microbarom frequencies as classical Bartlett and PMCC type methods fall short due to biases.	Accepted	This has been addressed in the conclusion. See point 9.
21	Line 53 Microseism modeling	Accepted	Microseism modelling was
22	Line 57 have been	Accepted	Have been
23	Line 57 Going back to the Garcés et al., 2004 study, I don't see any modeled microbaroms. The authors did compare observations with wind directions at different altitudes.	Accepted	The sentence has been deleted.
24	Line 61 operational	Accepted	
25	Line 64 Northern	Accepted	
26	Line 64 It is not at all clear that high-resolution atmospheric sounding methods	Accepted	This has been suppressed.

	would improve microbarom observations; as the wavelengths of microbaroms are large (1.7 km), it is only sensitive to the larger scale structure that is well captured in atmospheric models. Moreover, the Hupe study does not provide evidence that the agreement actually gets better. I would like the authors to address this.		
27	Line 66 explain how you extend the method and what the point is of this paper.	Accepted	This has been clarified.
28	Line 68 includes both seismic and infrasound arrays.	Accepted	both seismic and infrasound arrays
29	Line 70 In contrast to the microseism work, the influence of bathymetry on microbaroms has only been studied theoretically. There is no data yet to support this claim. Please describe this as such. Something like, "A recently modeling study by De Carlo (2020) suggests that bathymetry has negligible impact on microbarom source strength in contrast to predictions from the model by Waxler (2007)".	Accepted	
30	Line 73 propagation angles through the atmosphere	Accepted	
31	Line 74 already stated above	Accepted	The sentence has been deleted.
32	Line 75 Rewrite. This sentence reads as if microbaroms are not affected by geometrical spreading and attenuation but by "the strong spati-temporal variation of the middle atmosphere". Indeed, in both cases the propagation conditions (propagation path with its geometrical spreading and attenuation) are determined by the medium properties (which are temperature/wind for infrasound and elastic parameters for seismic waves). In the case of seismic waves, these medium properties do not vary in time.	Accepted	This has been clarified.
33	Line 75 Microseism modeling should also be considered in this paper; it would make the story much stronger as both waveform technologies are compared.	Accepted	The microseism predictions is considered. This is done via the addition of Figures 12 – 14. The predictions calculation is described in the methods section. The results are discussed in the section results and discussions.

34	Line 80 After reading this section, it is not clear to me what this paper adds to the existing knowledge. This should be stated, for example in the forelast paragraph.		This has been clarified. See point 1.
35	Line 80 studies	Accepted	
36	Line 80 I count four in Figure 1? From reading the manuscript, it looks like you have not plotted BVAR.	The BVAR is added to figure 1. There are 5 now.	Figure 1 is changed
37	Line 85 not relevant for scientific paper.	Accepted	The sentences are deleted.
38	Line 85 and	Accepted	and
39	Line 91 which type?	Accepted	Model 25
40	Line 92 double	Accepted	Deleted
41	Line 93 This station is not used so it is irrelevant to mention.	Accepted	Deleted
42	Line 94 discriminating between	Accepted	between
43	Line 97 consists of	Accepted	Consists of
44	Line 98 in a	Accepted	In a
45	Line 98 It appears to me that Figures 1, 2, 4, and 5 can be combined to show the overview map and the array layouts in one single figure. This will reduce the large number of figures in this paper (15). Alternatively, the seismic arrays can be combined similarly as Figure 2 for infrasound. It would be useful to plot the seismic arrays in Cartesian coordinates so that the array layouts can easily be compared to the infrasound arrays (Figure 2).	Accepted	The figures are combined into the new version of figure 1.
46	Line 98 Manufacturer?	Accepted	Guralp CMG-3v, also Geotech Instruments GS-21 at the line 101
47	Line 99 Figure 6 suggests that it is a broadband sensor.. why would it be at the edge of the response?	Accepted	This has been clarified.
48	Line 99 sensor's	Accepted	
49	Line 100 The ABKAR	Accepted	
50	Line 101 Figure 5	Accepted	Deleted
51	Line 101 a flat	Accepted	
52	Line 103 Perhaps better to show the frequency response with a logarithmic x-axis and include higher frequencies so that you can show the behavior of the GS-21 sensors above 1 Hz.	Accepetd	Figures 2 and 3 have been modified

	More realistic / smoother response plots will result from more points in the calculation of the response curves.		
53	Line 107 This point is an important added value of the paper and should be brought out in a revised version. Comparisons of co-located seismic and acoustic arrays would be novel.	Accepted	This has been highlighted in the introduction.
54	Line 113 Similar processing configurations should be used, including the same frequency band and window lengths.	Accepted	This setting for seismic processing has been chosen as it yields more stable detection results compared with the log-scaling configuration used for microbaroms. Further studies are needed to investigate the most suitable processing scheme as addressed in the conclusion.
55	Line 116 The authors should include array response functions and estimate for all arrays so that the resolution can be estimation from the lobe width.	Accepted	This has been addressed in the conclusion as further work to estimate realistic uncertainties in the wave parameter estimates.
56	Line 118 Can you explain the calculations more? The errors are quite dependent on SNR conditions and it may be that the current estimates are slightly optimistic, if for example a sigma_tau of 0.05 s is chosen (following Szuberla & Olson, 2004). Another way of looking at this is to consider the array response function and consider the lobe width.	Accepted	This has been mentioned. See point above.
57	Line 123 Microbarom sources are	Accepted	
58	Line 124 which frequency band is considered?		This has been clarified.
59	Line 127 scenarios	Accepted	
60	Line 127 using the high-resolution forecast (HRES) that is part of ECMWF's Integrated Forecast System (IFS) cycle 38r2	Accepted	using the high-resolution forecast (HRES) that is part of ECMWF's Integrated Forecast System (IFS) cycle 38r2
61	Line 130 Good is qualitative. Can you further quantify this? Within how many standard deviations can the model explain the data, for example?	Accepted	Quantitative measures are given.
62	Line 131 Results should not be part of the methods section.	Accepted	Deleted
63	Line 132 This interpretation should be saved for the discussion and not be part of the methods section.	Accepted and deleted as the same is stated again in the discussion section.	

	Moreover, it should be supported by data, for example by looking at variations in the effective sound speed along the various great circle paths that are studied. It should also be investigated what the differences in distance for a "southern" vs. "N. Atlantic source" would be.		
64	Line 134 Looking ahead at the observations, it seems like sources are more distributed in the south. There are two things to consider: (1) From the array processing perspective: As PMCC cannot detect more than one microbarom source per time-window, it could be that the resolution of such microbaroms is limited. This motivates the use of high-resolution methods such as discussed by den Ouden et al., 2020. (2) From the propagation perspective, there could be multiple paths/ducts from which microbarom energy can reach the array, leading to the observations of multiple infrasound sources (e.g., Assink et al., 2014). Thus, the paradigm of only observing propagation down-wind is challenged at microbarom frequencies.	Accepted	As suggested, explanations are given in the conclusion. See also point 20.
65	Line 143 Separate microbarom and microseism observations in two subparagraphs, this will make it easier to read.	Accepted	The paragraph was separated on two subparagraphs: 1.3.1 Source modeling for microbaroms and 1.3.2 Source modeling for microseisms
66	Line 143 Start with 2.1.1: microbaroms	Accepted	
67	Line 144 suggest rephrase: Figures 7 through 9	Accepted	
68	Line 145 suggest rephrase: of the dominant microbarom signals for infrasound arrays IS31, KURIS and MKIAR, respectively.	Accepted	of the dominant microbarom signals for infrasound arrays IS31, KURIS and MKIAR, respectively.
69	Line 145 suggest rephrase: The amplitudes and back azimuths from the dominant microbarom signals are selected from the PMCC bulletins and are plotted as orange dots.	Accepted	The amplitudes and back azimuths from the dominant microbarom signals are selected from the PMCC bulletins and are plotted as orange dots.

70	Line 147 Save this for the modeling paragraph.	Accepted	Deleted
71	Line 148 back azimuths	Accepted	
72	Line 153 azimuthal ranges of	Accepted	
73	Line 154 the KURIS	Accepted	
74	Line 154 shows	Accepted	
75	Line 155 Is there a reason why amplitudes would not increase to 0.1 Pa?		We have no explanation.
76	Line 157 Discuss how these distributions are computed	Accepted	This is the standard deviation around the dominant detected azimuths
77	Line 158 Suggest to have this in 2.1.2: microseisms	Accepted	
78	Line 161 rephrase. A 'detection system' is not appropriate.	Accepted	reworded
79	Line 161 Same.	Accepted	Same
80	Line 164 Is this related to the larger aperture of Kurchatov Cross and the loss of coherency? Can you identify a shift in frequency from winter to summer?	Accepted	This could be explained by higher noise level or a loss of signal coherency. We don't see clear shift in frequency from summer to winter.
81	Line 168 could this be related with the southern location of these arrays?	Accepted	This is suggested.
82	Line 173 can you explain why MKAR shows so much scatter, relatively?		We have no explanation.
83	Line 173 Can you explain why the Kurchatov array appears noisier than the other sites? Perhaps because the seismometers are not installed in boreholes? Or is it related to the instrument? The amplitudes also seem higher than the other sites. Can you adjust the vertical scale so that all are equal?	Accepted	The vertical scale is adjusted.
84	Line 175 The microbaroms simulations have been computed for the sea states around the infrasound arrays, not for the microbarom recordings. Please provide more detail about the computation, which distances are considered? Are very low amplitudes cut off from the computation? There is a large difference between the simulations and observations in the summer at all arrays.	Accepted	The back-azimuths and amplitudes have been calculated for the expected microbarom sources at IS31, KURIS, and MKIAR. The expected distances to the source regions vary with season. For example at IS31, simulations predict in winter three source regions (Figure 6 a); distances to North Atlantic regions range between 3500 to 7000 km while the distance to the North Pacific region is around 7000 km. In summer, additional microbarom sources are located in the southern hemisphere at distances larger than 11000 km (Figure 6 b).

85	Line 175 Figures 7 through 9	Accepted	Figures 8 through 10
86	Line 176 This, in a way, is not so spectacular, given the large distance to this source, making it appear to come from one dominant azimuth. I would discuss that the scatter of microbarom sources tells something about the relative distance to the source. This can also be seen in Den Ouden et al.,2020 (compare for example IS42 with IS48).		We think that the relation between the scattering and the relative distance to the source is not clear, as large scattering is also noted for the farthermost source regions in the southern hemisphere.
87	Line 178 Can you quantify the deviation?	Accepted	
88	Line 182 I note that the model that is used for microbarom modeling could indeed be used to simulate microseisms. Please explain why amplitudes need an emperical factor and do not follow from the physics. Furthermore, does this mean that amplitude is a free parameter?	Accepted	As the used source model was developed for microseisms (Ardhuin et al., 2011), an empirical scaling factor (F = 1:10000) has been applied to account for wave coupling effect in the atmosphere, thus allowing qualitative comparisons between the observed and predicted temporal variations of the microbarom amplitudes.
89	Line 185 could one not equally argue that summer amplitudes are correct while winter amplitudes are underestimated?		We believe that microbarom modeling is not correct for long propagation range as atmospheric model taken at the station likely predicts more favorable propagation conditions compared with situation involving waves crossing the equator line.
90	Line 188 where would these sources be? please further explain. It would be good if a Figure would be devoted to microbarom / microseism sources during summer and during winter.	Accepted	Figures 6 and 7 are devoted to the microbarom and microseism sources accordingly. The descriptions are in the methods section.
91	Line 191 I would like the authors to discuss the shortcomings in the current method (data processing, range-independence) in a revised version of the manuscript.	Accepted	This study provides a first characterization of the seasonal patterns of microbarom and microseisms recorded by the IGR seismo-acoustic network. The chosen detection algorithm and propagation model offer a good trade-off between low calculation effort and propagation accuracy. Identified shortcoming is the limitation of PMCC to detect overlapping microbarom sources originating from different directions. Furthermore, the approach assuming range-independent atmosphere may lead to erroneous interpretations for situations involving long propagation ranges where significant along-path variability of wind and temperature profiles may occur, in particular when modeling the relative strength of microbarom sources located in different hemispheres. This has been clarified in the manuscript.

92	Line 194 Explain how the number of detections can be quantified and be directly compared to a simulated value. Are the number of detections averaged over 6 hours to be directly compared with the simulations? What is the role of wind noise?	Rejected, misunderstanding is a result of mistranslation. The translation was improved.	Figure 15 shows the azimuthal distribution of infrasound detections having the maximum amplitudes.
93	Line 198 Repeat from above: Looking ahead at the observations, it seems like sources are more distributed in the south. There are two things to consider: (1) From the array processing perspective: As PMCC cannot detect more than one microbarom source per time-window, it is likely that the ability to resolve microbaroms is limited and biased. This motivates the use of high-resolution methods such as discussed by den Ouden et al., 2020. (2) From the propagation perspective, there could be multiple paths/ducts from which microbarom energy can reach the array, leading to the observations of multiple infrasound sources (e.g., Assink et al., 2014). Thus, the paradigm of only observing propagation down-wind is challenged at microbarom frequencies.	Accepted.	We agree with this limitation. This has been clarified in the conclusion. See also points 20 and 64.
94	Line 206 I suppose this is identified using trace velocity. Could the authors clarify?	Yes, it is true.	These peaks could likely be explained by body and surface seismic phases judging by its trace velocity.
95	Line 214 Please include information the typical distances to microbarom/microseism sources and a map showing the typical locations of sources that are likely to be detected.	Accepted	The maps are in figure 6 and 7
96	Line 228 given the large number of assumptions in this paper, I would be careful with placing the inaccuracy with the ECMWF model.	Accepted	We suppressed this statement.
97	Line 231 This would rather be a transient signal; how would that lead to such a large mismatch?	Accepted	We suppressed this statement.
98	Line 237 please provide evidence for this statement.	Accepted	The sentence has been reworded.

99	Line 239 During minor SSWs, bi-directional conditions may occur which may have strong impacts on the retrieved microbarom signals (see Assink et al., 2014; JGR).	Accepted	This has been added.
100	Line 243 but the wavelength is also 10 times larger, so I cannot imagine how the azimuthal errors would decrease. this also assumes that microbaroms and microseisms originate from the same location.	Accepted	The sentence has been suppressed.
101	Line 389 BVAR is not plotted	Accepted	
102	Line 411 - Make the vertical size larger so you can see more detail. - Include more tick marks for the back azimuth values.	Accepted	The vertical size is enlarged. A bigger amount of the tick marks are included.
103	Line 418 - Make the vertical size larger so you can see more detail. - Include more tick marks for the back azimuth values.	Accepted	The vertical size is enlarged. A bigger amount of the tick marks are included.
104	Line 421 - Make the vertical size larger so you can see more detail. - Include more tick marks for the back azimuth values.	Accepted	The vertical size is enlarged. A bigger amount of the tick marks are included.
105	Line 427 Can you make the y-axis scale the same?	Accepted	Y-axis scales are made uniform.
106	Line 432 Can you make the y-axis scale the same?	Accepted	Y-axis scales are made uniform.

Formatted: English (United States)

Characterizing the global ocean ambient noise as recorded by the dense seismo-acoustic Kazakh network

Alexandr Smirnov[1,2], Marine De Carlo[3], Alexis Le Pichon[3], Nikolai M. Shapiro[2,4,5], Sergey Kulichkov[6]

[1]Institute of Geophysical Research, Almaty, 050020, Kazakhstan
[2]Institut de Physique du Globe de Paris, Sorbonne Paris Cité, F-75005 Paris, France
[3]CEA, DAM, DIF, F-91297 Arpajon, France
[4]Institut de Sciences de la Terre, Université Grenoble Alpes, CNRS (UMR5275), Grenoble, France.
[5]Schmidt Institute of Physics of the Earth, Russian Academy of Sciences, Moscow, Russia
[6]A.M. Obukhov Institute of Atmospheric Physics RAS, Moscow, 119017, Russia

Correspondence to: Alexandr Smirnov (smirnov@ipgp.fr)

Abstract. The dense seismo-acoustic network of the Institute of Geophysical Research (IGR), National Nuclear Center of the Republic of Kazakhstan, has been operating in Kazakhstan since the late nineties of the last century. It consists of five seismic and three infrasonic arrays. The IGR network includes stations that are part of several national and global monitoring systems. Infrasonic and seismic data are processed using the Progressive Multi-Channel Correlation (PMCC) detector to characterize the temporal variability of microbarom and microseism signals from 2014 to 2017. The non-linear interaction of ocean waves is simulated using the microseism source model distributed by the French Research Institute for Exploitation of the Sea (IFREMER). The wave attenuation is calculated using a semi-empirical propagation law in a range independent atmosphere. The observed and predicted infrasonic and seismic signals are compared, confirming a common source mechanism for both microbaroms and microseisms. This study reveals the dominating directions of arrivals at each station of the IGR network and the associated source regions. Multi-year and intra-seasonal parameter variations are analysed, revealing the strong influence of long-range atmospheric propagation on microbarom predictions. In winter, dominating sources of microbaroms are mainly located in the North Atlantic and in the North Pacific during Sudden Stratospheric Warming (SSW) events while signals observed in summer likely originate from source regions in the southern hemisphere.

Deleted: 91680
Formatted: French (France)
Formatted: English (United Kingdom)
Deleted: four
Formatted: English (United States)
Deleted: Comparing
Deleted: t
Deleted: seismic and infrasonic signals
Deleted: reveals the dominating directions of arrivals at each station of the IGR network and the associated source regions. Both multi-year and intra-seasonal parameter variations are analysed. The level of low-frequency noise is significantly higher in winter than in summer.
Deleted: infrasound ambient noise
Deleted: . S
Deleted: ,
Deleted: ing
Deleted: , are discussed

Introduction

Pressure fluctuations of ocean infra-gravity gravity waves are primarily at the origin of seismic ambient noise categorized as seismic hum (1–20 mHz), primary microseisms (0.02–0.1 Hz), and secondary microseisms (0.1-1 Hz). The theory to predict microseisms and microbarom source regions was developed by Longuett-Higgins (1950). This theory explains how counter propagating ocean waves can generate propagating acoustic waves and create secondary microseisms by exciting the sea floor. Gutenberg (1953) first pointed out the relation between microseisms, meteorological conditions, ocean waves, and microbaroms. Hasselmann (Hasselmann, 1963, 1966) generalized Longuett-Higgins' theory to random waves by investigating non-linear forcing of acoustic waves. Donn and Naini (1973) suggested a common source mechanism of microbaroms and microseisms from the same ocean storms demonstrating that the only mechanism capable of transmitting energy into both the atmosphere and the sea bottom is associated with the surface waves in a storm area. Microseism modelling was introduced by Kedar et al. (2008). The good correlation between the observed microseism amplitudes and their predicted values according to the Longuett-Higgins theory was shown, demonstrating that microseism source locations can be tracked using numerical modeling (Shapiro, 2005; Shapiro and Campillo, 2004; Stehly et al., 2006; Stutzmann et al., 2012; Weaver, 2005).

A radiation model of microbaroms from the motion of the air/water interface was later proposed by Waxler and Gilbert (2006). Ardhuin and Herbers (Ardhuin and Herbers, 2013a) developed a numerical model based on Longuett-Higgins-Hasselmann theory for the generation of Rayleigh waves, considering an equivalent pressure source at the undisturbed ocean surface. The different patterns between microseismic body and surface waves resulting from distinctive amplification of ocean wave-induced pressure perturbation and different seismic attenuation have been studied with implications for seismic imaging and climate studies (Obrebski et al., 2013). Coastal reflections also play an important role in the generation of microbaroms and microseisms but modelling the reflection of ocean waves off the coast still remains a major source of model uncertainty (Ardhuin et al., 2013b).

As for microseisms, microbaroms are not the impulsive signals but quasi-monochromatic sequences of permanent waves (Olson and Szuberla, 2005); therefore, it is not possible to detect their onset and identify their propagation paths. However, these signals are well detected using standard processing techniques, such as beamforming methods used from the sixties (Capon, 1972; Haubrich and McCamy, 1969; ToksoZ and Lacoss, 1968). Several studies demonstrated the efficiency of beamforming approaches (e.g. Evers and Haak, 2001) or correlation-based methods (e.g. Garcès, 2004; Landès et al., 2012) to detect and characterize microbarom signals globally. ;

The microbarom frequency band is at the lower edge of the frequency band of interest to monitor nuclear tests. Recent global scale microbarom observations recorded by the International Monitoring System (IMS) network of the Comprehensive Nuclear Test Ban Treaty Organization (CTBTO) confirm that its detection capability is highly variable in space and time (Ceranna et al., 2019). Thus, in order to assess the microbarom source intensity accurately, it is necessary to take into account a realistic description of the middle atmosphere. Other studies have been conducted to characterize the ambient infrasound noise. Smets et al. (2014) compared three months of microbarom observations with the expected values to study the life cycle of Sudden Stratospheric Warming events. Landès et al. (2014) compared the modelled source region with microbarom observations at operational IMS stations. Le Pichon et al. (2015) compared observations and modelling over a 7-month period to assess middle atmospheric wind and temperature models distributed by European Centre for Medium-Range Weather Forecasts (ECMWF).

Deleted: this

Deleted: ,

Deleted: resulting acoustic frequency is twice the frequency of the ocean waves

Deleted: ,

Deleted: such

Commented [ALP1]: Check name, strange spelling..

Deleted: More

Deleted: ; Hupe et al., 2018

Deleted: .recent algorithms are efficient

Deleted: continuous and global

Deleted:

Deleted: (Evers and Haak, 2001

Formatted: English (United Kingdom)

Deleted: The above mentioned studies were conducted using IMS infrasound data as well as infrasound records from national networks (e.g. KNMI network, Evers and Haak, 2001).

Deleted: nuclear

Deleted: 8

Deleted: were

Deleted: operating

More recently, Hupe at al. (2018) showed a first order agreement between the modelled and observed microbarom back-azimuth and amplitude in the Northern Atlantic.

In this paper, we further extend the approach developed by Hupe at al. (2018) by densifying the monitoring network. The considered dense seismo-acoustic Kazakhstani network is operated by the Institute of Geophysical Research (IGR) of the National Nuclear Center of the Republic of Kazakhstan and includes both seismic and infrasound arrays. Using such experimental setting, we aim at developing synergetic approaches to better constrain microbarom source and evaluate propagation effects. Since the pioneer work of Donn and Naini (1973), this study is to our knowledge the first multi-year comparisons between observed and modelled microbaroms and microseisms at co-located seismo-acoustic arrays.In the first part, we present the observation network and methods used in this study. In the second part, the processing and modelling results of microseism and microbarom signals recorded by the IGR seismo-acoustic network from 2014 to 2017. In the last part, comparisons between microbarom predictions and observed microbaroms and microseisms signals are discussed.

1 Observation network and methods

1.1 Observation network

The Kazakhstani seismo-acoustic network (KNDC, 2019) is unique for microbarom and microseism studies, as it contains a five seismic and three infrasound arrays (Figure 1).

The infrasound network consists of the IMS infrasound station IS31 located in north-west Kazakhstan (2.1 km aperture, 8 elements), two national arrays of 1 km aperture: KURIS (4 elements) near the Kurchatov and MKIAR (9 elements) near the Makanchi village (Belyashov et al., 2013) (Figure 1). KURIS and MKIAR have been operating since 2010 and 2016, respectively. Microbarometers MB2000 and MB2005 are used at IS31 and KURIS, and Chaparral Physics Model 25 microbarometers are installed at MKIAR. Figure 2Figure 3 shows the frequency response of the microbarometers. These stations form a unique dense regional infrasound network. Combining infrasound observables recorded by this network allows discriminating between regional natural and anthropogenic sources (Smirnov, 2015; Smirnov et al., 2011, 2018).

The seismic network consists of Kurchatov Cross array and MKAR part of the IMS network, ABKAR and KKAR part of the Air Force Technical Applications Center (AFTAC, USA) network (Figure 1 and Table 1). The Kurchatov cross array consists of 20 elements arranged in a cross with an aperture of 22 km (Figure 1). It consists of Guralp CMG-3V sensors. While in the 0.1-0.3 Hz band, MKAR, ABKAR and KKAR sensors are at out of the frequency band of interest (0.1-0.3 Hz), the frequency response of the Kurchatov cross array is flat within the secondary microseismic band. The configuration of ABKAR, BVAR, KKAR and MKAR are similar with nine elements and an aperture of ~5 km. The ABKAR array configuration is shown as callouts in Figure 1Figure 5. These arrays are equipped with Geotech Instruments GS21 short period vertical sensors with a flat response for frequencies above 1 Hz. Figure 3Figure 6 shows the frequency response of GS-21 and CMG-3V sensors within the frequency range of 0.1-0.4 Hz. Surface waves from the ocean storms are well recorded by broad band seismometers.

Deleted: These agreements have been improved using more accurate wind profiles obtained from high resolution LIDAR middle atmospheric sounding (Hupe et al., 2018).

Deleted: using microbarom recorded

Deleted: by the dense Kazakhstani network

Deleted: This

Deleted: network

Deleted:

Deleted: not only infrasound but also seismic arrays

Deleted: With

Deleted: this network

Deleted: can be used to

Deleted: ¶

Deleted: study

Deleted: Stations in the network are part of other global networks such as the IMS (CTBTO), IRIS consortium, etc. KNDC closely cooperates with the institutions responsible for these networks and leading seismic and infrasound centers such as the International Data Center (IDC, Austria) of the CTBTO, AFTAC and Commissariat à l'Energie Atomique (CEA, France).

Deleted: in

Deleted: ,

Deleted: , and

Deleted: in

Deleted: callouts at the (Figure 2

Deleted:)

Deleted: Figure 3

Deleted: MB2000

Deleted: The frequency responses of other sensors are flat from 0.01 to 5.0 Hz. Together with the IMS station IS46, t

Deleted: differs from the others with

Deleted: as a

Deleted: callout at the

Deleted: (Figure 4)

Deleted: Although

Deleted: frequency

Deleted:

Deleted: is

Deleted: the

Deleted: edge of the sensor's frequency response, they can record

Deleted: s

Deleted: Figure 5

Deleted: Figure 6

Body waves are also registered on GS21 short period sensors. Although, in the frequency band of interest the signal attenuation is about 30 dB, all stations detect microseisms effectively due to their large amplitude above the background noise. A peculiarity of the network is that infrasound and seismic arrays are collocated at two sites (KURIS and Kurchatov Cross; MKIAR and MKAR) or installed relatively close to each other (IS31 and ABKAR are 220 km apart, Figure 1). Figure 4 and Figure 5 show typical power spectral density (PSD) of the ambient noise for the infrasound and seismic arrays, respectively. The PSD calculation was carried out using one-hour time window during calm periods on October 23 and July 15. The microbarom peak clearly appears at all infrasound arrays only in October. In the summertime, this peak is visible only at IS31. As opposed to the infrasound noise, the seismic noise spectra exhibit the microseismic peak in both seasons with an overall noise level in October approximately 10 dB higher than in July. This effect is most pronounced at the Kurchatov Cross array.

1.2 Processing method

Microseisms are detected using the Progressive Multichannel Correlation Method (PMCC) (Cansi, 1995; Cansi and Klinger, 1997; Smirnov et al., 2011) in 10 linearly spaced frequency bands between 0.05 and 0.4 Hz. A fixed time window length of 200 s is used for each sub-band. For infrasound processing, the frequency band is broadened to 0.01-4 Hz using fifteen logarithmically scaled sub-bands, and time window length varying from 30 s to 200 s (Matoza et al., 2013). Only detections with a mean frequency ranging in the 0.1–0.4 Hz microbarom band are considered.

It is important to take into account uncertainties in azimuth and apparent velocity estimations identified in microbarom studies. The uncertainties of the estimated wave parameters of microseisms can be large due to the relatively small aperture of the seismic arrays. Uncertainties in wave parameter estimates are calculated considering the array geometry of the above mentioned infrasound and seismic arrays (Szuberla and Olson, 2004) (Table 1). For the infrasound arrays, the horizontal velocity is set to 340 m/s. For the seismic arrays, the value of 3000 m/s is chosen corresponding to the average speed of the Rayleigh wave. The uncertainties for the seismic arrays are significantly higher for the body waves due to higher velocities. It should be noted that these errors are optimistic as the estimation do not take into account site and time dependent signal-to-noise ratio.

1.3 Source modelling

Sources of microseisms are distributed by IFREMER (IFREMER, 2018) referred to as ‘p2l’ – as a composite calculated from the wave-action WaveWatch III model (WW3) developed by the National Oceanic and Atmospheric Administration (NOAA). While the bathymetry strongly affects the source intensity in microseism modelling (Ardhuin et al., 2011; Ardhuin and Herbers, 2013a; Kedar et al., 2008), a recently modeling study by De Carlo (2020) suggests that bathymetry has negligible impact on microbarom source strength in contrast to predictions from the model by Waxler (2007). In this study, the source term at the ocean surface for microseisms (‘p2l’) which does not include coupling with the bathymetry is taken as a proxy to model microbaroms). To model microbarom signals, the WW3 wave action model developed by NOAA and distributed by

Deleted: (0.1-0.3 Hz),
Deleted: ¶ Figure 4
Deleted: s
Deleted: the
Deleted: noise
Deleted: and Figure 5 Figure 5 shows the same for the seismic stations
Deleted: on the
Deleted: one-hour-long interval of the
Deleted: record
Deleted: m
Deleted: the records of the
Deleted: in the
Deleted: records
Deleted: T
Deleted: for the seismic stations differ strongly from that on ...
Deleted: appears clearly
Deleted: . However, it should be noted that the
Deleted: is
Deleted: in the records of the
Formatted: English (United States)
Formatted: English (United States)
Formatted: English (United States)
Formatted: English (United States)
Formatted: English (United States)
Formatted: English (United States)
Formatted: English (United States)
Formatted: English (United States)
Formatted: English (United States)
Formatted: English (United States)
Formatted: English (United States)
Formatted: English (United States)
Formatted: English (United States)
Formatted: Normal
Deleted: These nonlinear interactions also generate waves ...
Deleted: microbaroms efficiently propagate at shallow propagat ...
Deleted: ,
Deleted: and
Deleted: are assumed identical (Ardhuin and Herbers, 2013; ...

IFREMER was used. While microseisms propagate through the static structure of the solid Earth, microbaroms are primarily affected by the strong spatio-temporal variability of the temperature and wind structure of the atmosphere. Therefore, the geometrical spreading and seismic attenuation are the main effects to account for microseism modelling (e.g. Kanamori and Given, 1981; Stutzmann et al., 2012), while the dynamical properties of the middle atmosphere should be taken into account for microbarom modelling.

1.3.1 Source modeling for microbaroms

Microbarom sources are computed following the approach developed by De Carlo et al. (2018, 2020). Simulations are carried out using the microbarom generation theory at the microseismic secondary peak (0.1-1 Hz) based on the non-linear oceanic wave interaction (Ardhuin and Herbers, 2013a). Input data are calculated over a global grid of resolution 0.5° in space and 6 hours in time. For the attenuation, we use a semi-empirical frequency dependent attenuation relation derived from massive parabolic equation simulations and consider realistic propagation scenarios. Atmospheric specifications are given by the high-resolution forecast (HRES) that is part of ECMWF's Integrated Forecast System (IFS) cycle 38r2 (Le Pichon et al., 2012). Atmospheric profiles are given at the station and are assumed to be constant along the propagation path. This approach shows overall first order agreement between microbarom observations and predictions generated in the northern hemisphere similar to those described by De Carlo et al. (2018) and Hupe et al. (2018) (in a range of ~10° for the back-azimuths).
The correlation coefficient between the observed and predicted seasonal patterns is calculated following metrics elaborated by Landès (Landès et al., 2014). There are two different metrics: (i) S_{corr_Az} which defines the correlation between the observed (N_{obs}) and predicted (N_{pred}) marginal detection number in the direction θ_{Amax} versus time (t):

$$S_{corr\_Az} = C_{corr}\left[N_{obs}(\theta_{Amax}, t), N_{pred}(\theta_{Amax}, t)\right] \quad (1)$$

and (ii) S_{corr_Amp} for the correlation between the predicted and observed amplitude A_{max}.

$$S_{corr\_Amp} = C_{corr}\left[N_{obs}(A_{max}, t), N_{pred}(A_{max}, t)\right] \quad (2)$$

Figure 6 shows the distribution of the epicenters of the expected microbarom sources from January to February 2017. The map shows regions of the globe from where signals recorded at IS31 with the largest amplitude originate. The calculation was carried out for two winter and two summer months. The distribution of the epicenters is not uniform, appearing as several aggregations shown on the maps as coloured surfaces according to the dominant frequencies of the predicted sources and expected amplitudes at the station. The digits on the map indicate the mean amplitude and frequency of the corresponding clusters.

1.3.2 Source modeling for microseisms

The bathymetry effect plays an important role when calculating the microseism source intensity. Longuet-Higgins (1950) showed that the pressure fluctuations do not attenuated with depth but are transmitted to the ocean bottom as acoustic waves.

Deleted: The bathymetry strongly affects the source intensity in microseism modelling (Ardhuin et al., 2011; Kedar et al., 2008); however, it has negligible impact on microbarom source strength (De Carlo et al., 2020). Microseisms propagate through the sea floor while Microbaroms are primarily affected by the temperature and wind structure of the atmosphere, whereas
Deleted: (Garcès, 2004).
Deleted:
Deleted: strong spatio-temporal variability
Deleted:
Deleted: ¶
Formatted: Font color: Auto
Formatted: Indent: Left: 1.27 cm
Deleted: I
Deleted: <#>¶
<#>The m
Formatted: Font color: Auto, English (United States)
Deleted: <#>model is
Deleted: <#>,
Deleted: <#> using
Deleted: <#>through the HRES IFS cycle 38r2 ECMWF ...
Deleted: specifications
Deleted: good
Deleted: results
Deleted: for
Deleted:
Deleted: However, such an approach does not explain the obser ...
Formatted: English (United Kingdom)
Formatted: English (United Kingdom)
Formatted: English (United Kingdom)
Formatted: English (United Kingdom)
Formatted: English (United States)
Deleted: 1
Formatted: English (United States)
Formatted: English (United States)
Deleted: I
Formatted: English (United States)
Formatted: English (United States)
Formatted: English (United States)
Formatted: Font: 10 pt
Deleted: Longuet-Higgins,
Deleted: are

Depending on the ratio between the wavelength of the acoustic waves and the ocean depth, resonance effects can occur leading to a modulation of the pressure fluctuations at the sea floor (Stutzmann et al., 2012). The corresponding seismic source power spectral density at the ocean bottom is:

$$S_{DF}(f_s = f_2) = \frac{2\pi f_s}{\rho_s^2 \beta^5} \left[\sum_{m=1}^{m=N} c_m^2\right] F_p(\mathbf{K} \cong 0, f_2 = 2f) \quad (3)$$

Equation (3) is derived from Longuet-Higgins equation (186). S_{DF} is in m/Hz, ρ_s and β are respectively the density and S-wave velocity in the crust. f_s is the seismic frequency which is equal to the pressure fluctuation frequency f_2 and it is the double of the ocean wave frequency f. Coefficients c_m correspond to the compressible ocean amplification factor. c_m are non-dimensional numbers which vary between 0 and 1 as a function of the ratio $2\pi f 2h/\beta$ where h is the water depth (Longuet-Higgins, 1950). Considering the crustal density ρ_s = 2600 kg m^{-3} and S-wave velocity β = 2800 m/s, Figure 7 shows the map of the sources of microseism distribution for ABKAR.

2 Results

2.1 Processing results

Signals from the ocean storms are successfully extracted from the records at all IGR infrasound and seismic arrays. Diagrams in this section show the back-azimuths of the signals as a function on time. Distributions of the maximum amplitudes are included as well. The amplitude maxima are found in the PMCC bulletins each 6 hours of the entire period of 2014-2017.

2.1.1 Microbaroms Signals from ocean storms recorded at infrasound and seismic arrays are successfully identified. Figure 8 to 10 show the temporal variation of the dominant microbarom signals for infrasound arrays IS31, KURIS and MKIAR, respectively. The amplitudes and back-azimuths of the dominant microbarom signals are selected from the PMCC bulletins and are plotted as orange dots.

The graphs show pronounced seasonal variations for both back-azimuths and amplitudes. The largest amplitudes are observed during the winter months, when signals with back-azimuths of 320±20° prevail (Figure 8). Few detections with back-azimuths of 35±15° are also detected in winter. During the summer months, low-frequency signals with back-azimuths of 210±50° dominate. In winter, the amplitudes range from ~0.001 to ~0.1 Pa, the largest values being observed in winter.

Figure 9 shows the observational data for KURIS. The back-azimuths measured at this station are similar to those recorded at IS31, with slightly higher values in winter (325±15°). In summer, two regimes are distinguished in the azimuthal ranges of 230±30° and 130±30°. Detections near 50° are also observed in winter. Similarly to IS31 data, KURIS data shows that maximum microbarom amplitudes are observed in winter. From summer to winter, the maximal signal amplitude increases from 0.001 to 0.03 Pa.

MKIAR started recording microbaroms in August 2016 with repetitive seasonal variations (Figure 10). One cluster of detections dominates in winter at ~330° and two clusters in summer at 230° and 110° with a corresponding standard deviation of ±10°, 25° and 25°, respectively.

Deleted: ocean bottom…ea floor (Stutzmann et al., 2012). TThe
Deleted: 2
Deleted: ….ation (2
Deleted: …z^{-1}… ρ_s and β are respectively the density and S-wave velocity in the crust. f_s is the seismic frequency which is equal to the pressure fluctuation frequency f_2 and it is the double of the ocean wave frequency f
Formatted: Font: 10 pt
Formatted
Deleted: $^{-1}$
Deleted: Figure 7
Formatted: Font: 10 pt
Formatted
Formatted: Font: 10 pt
Deleted: . the map is calculated …or the …BKAR seismic array
Formatted: Normal
Deleted: of…t all the …GR infrasound and seismic arrays. Diagrams in this section show the back-azimuths of the signals as a function on time. Distributions of the maximum amplitudes on time are included as well. The amplitude maxima are found in the PMCC bulletins each 6 hours of the entire investigation
Deleted: ¶
Deleted: Figure 8Figure 7…,
Formatted: English (United States)
Formatted: English (United States)
Deleted: through
Formatted: English (United States)
Deleted: Figure 9Figure 8 and Figure 10Figure 9
Deleted: …zimuths from
Deleted: of the azimuths of signals with maximum amplitudes extracted from the PMCC bulletins for each six-hour interval between 2014 and 2017.…Figure 7 shows the results for station IS
Deleted: In addition to these results, the expected microbarom
Formatted
Deleted:
Formatted: English (United States)
Formatted: English (United States)
Deleted:
Deleted: Figure 9Figure 8… shows the observational data for
Deleted: the
Deleted: repeatable
Deleted: Figure 10Figure 9
Deleted: system …ominates in winter at ~330°±10° is observed

2.1.2 Microseisms

Figure 11 shows results for ABKAR seismic array. In addition to the observations, the diagrams represent the simulated microseism parameters. Amplitudes are the largest in winter where detections with back-azimuths of 340±20° prevail. During summer months, signals with back-azimuths of 290±20° dominate. The amplitudes range from ~0.4 to ~20 nm/s varying from the largest values in winter to minimum values in summer. Figure 12 shows results for KKAR. Two clusters of detections at 330±20° and 5±5° is observed in winter while in summer there are clusters at 160±20° and 190±15°. The seasonal amplitude variation is 0.5-7.0 nm/s. Figure 13 shows the results for Kurchatov Cross. In winter, back-azimuths of microseisms are 300±20°. A small amount of signals with 50±50° is observed in summer. Amplitudes reach their maximum in winter and minimum in summer, ranging from 8 to 200 nm/s. This is significantly higher than for all other arrays because Kurchatov Cross array is equipped with broad-band seismometers while all the other arrays register signals with short period sensors, showing amplitude frequency response falloff within the surveyed frequency range. Figure 14 shows results for MKAR. Two clusters at 310±20° and 5±5° are observed in winter while in summer there are clusters at 130±10° and 180±10°. The seasonal amplitude variation is 0.7-7.3 nm/s. The seasonal trend of the maximum microseism amplitudes recorded at all seismic stations is similar, with a maximum observed in winter. At MKAR and KKAR, microseism amplitudes are characterized by a slight increase in the middle of summer which could be related with the southern location of these arrays. Such a peak is not observed at ABKAR. At the Kurchatov Cross station, there are a small amount of detections in summer which could be explained by higher noise level or a loss of signal coherency at this site. The graphs clearly show that the amplitudes vary synchronously even at smaller time scale (Figure 17). However, a decrease in amplitude is observed early January 2017 at all stations. As expected, the maximum amplitudes in winter decrease with increasing distance from the stations to the North Atlantic region (about 10, 8, and 4 nm/s for ABKAR, KKAR, and MKAR, respectively). At Kurchatov, the amplitude is significantly higher in winter (in the order of 80 nm/s).

2.2 Modelling results 2

The back-azimuths and amplitudes have been calculated for the expected microbarom sources at IS31, KURIS, and MKIAR. The expected distances to the source regions vary with season. For example at IS31, simulations predict in winter three source regions (Figure 6 a); distances to North Atlantic regions range between 3500 to 7000 km while the distance to the North Pacific region is around 7000 km. In summer, additional microbarom sources are located in the southern hemisphere at distances larger than 11000 km (Figure 6 b). Figure 8 to 10 compare the observed and predicted arrivals at these stations. During winter months, a good agreement is found: IS31 records microbaroms with back-azimuths of 320±20° within the predicted range (Figure 8 a and c). A good agreement is also observed at KURIS (Figure 9 a, c) and MKIAR (Figure 10 a, c). During the summer months, the agreement in azimuths remains satisfactory at all stations within a range of ±30°. IS31 records microbaroms within 210±50° with a slight shift compared with the predicted system (185±50°). At KURIS, the observed systems 230±30° and 130±30° are different compared with the predicted ones (±10° and 160±10°). At MKIAR, during the

Formatted: English (United States)

Formatted: English (United States)

Deleted: highest

Deleted:

Deleted: of detections

Formatted: Font: Not Bold

Formatted: Font: Not Bold

Formatted: Font: Not Bold

Deleted: As for microbaroms, microseism systems are extracted in the 0.1-0.4 Hz band within a six-hour interval time window from January 1, 2014, to December 31, 2017. Figure 10 shows the azimuths of low-frequency signals at four seismic IGR stations: (a) ABKAR, (b) KKAR, (c) Kurchatov Cross, and (d) MKAR stations. In winter, the graphs show similar features at all stations. A dominant detection system corresponds to signals from northwestern and northern directions. Other systems are identified: 340±15° (ABKAR), 350±25° (KKAR), 305±15° (Kurchatov Cross), and 320±10° and 5±5° (MKAR). In summer, the situation varies from one station to another. At ABKAR, one system at 290±15° is observed. At KKAR and MKAR, two systems with azimuths of 160±20°, 90±15° and 190±10°, 145±15°, respectively, are distinguished. Finally, at Kurchatov Cross array, it is impossible to identify a prevailing direction in summer. Figure 11 shows the maximum amplitudes at the four seismic arrays. ¶
The seasonal trend of the maximum microseism amplitudes recorded at all seismic stations is similar, with a maximum observed in winter. At MKAR and KKAR, microseism amplitudes are characterized by a slight increase in the middle of summer which could be related with the southern location of these array ...

Formatted: Indent: Left: 1.27 cm

Deleted: . ¶

Formatted: Font: Not Bold

Formatted: Font: Not Bold

Deleted: Modelling results

Deleted: Expected The back-azimuths and amplitudes have been ...

Formatted: Highlight

Formatted: Highlight

Formatted: Highlight

Deleted: The back-azimuths and amplitudes have been calculate ...

Deleted: Figure 7

Deleted: , Figure 8 and

Deleted: Figure 9through

Deleted:

Deleted: simulated

Deleted: Figure 7

Deleted: Figure 9Figure 8

Deleted: Figure 10Figure 9

summer months, microbaroms within the predicted range of 60-270° are consistent with the observed systems (230±25° and 110±25°). As the used source model was developed for microseisms (Ardhuin et al., 2011), an empirical scaling factor (F = 1:10000) has been applied to account for wave coupling effect in the atmosphere, thus allowing qualitative comparisons between the observed and predicted temporal variations of the microbarom amplitudes. At all stations, there is good agreement between the predicted and observed amplitudes during the winter months (Figure 8 d, Figure 9 d and Figure 10 d), but in summer the predicted amplitudes are overestimated when compared to the observed ones (Table 2).

To summarize, both amplitudes and azimuths are well predicted in winter as opposed to summer months. The observed discrepancies are explained here by unrealistic simulated wave attenuation for dominating sources located in the southern hemisphere due to the assumed range independent atmosphere. Quantitative estimations of the prediction quality (S_{corr} calculated according to equations (1) and (2)) are summarized in Table 2.

3 Discussions

Where previous studies analysed microbarom signals at a single station (Hupe et al., 2018), further investigations are conducted in this study by considering a multi-year dataset of continuous records collected by the IGR network. Regional features of both microbaroms and microseisms are highlighted.

Figure 15 shows the azimuthal distribution of infrasound detections having maximum amplitudes. The histograms of the azimuthal distribution of microbaroms clearly show the dominating direction of arrivals in winter with prevailing directions ranging from 270 to 350° (Figure 15 b). The predicted azimuths are in good agreement with the observed ones (Figure 8 c, Figure 9 c, Figure 10 c, Figure 15 b and Table 2). Observations, as well as simulations, show large temporal variations in the dominating microbarom source regions explained by the seasonal reversals of the prevailing stratospheric winds, which in turn, cause the migration of storm activity area to the winter hemisphere (Stutzmann et al., 2012).

Figure 16 shows similar histograms for seismic stations. One can distinguish seasonal trends for both infrasonic and seismic observations. In winter, microbaroms and microseisms are detected from northern and north-western directions (Figure 15 b and Figure 16 b). In summer, southern, southwestern and south-eastern directions dominate (Figure 15 c and Figure 16 c). Signals from north-western direction are also recorded at ABKAR, KKAR, and MKAR in summer. Azimuths differ from one station to another depending on the strongest microbarom and microseism source regions relative to the station locations. As for microbaroms, during winter months, microseism observations exhibit a similar pattern with a larger spreading (250-360°), and an additional peak (0-20°) at KKAR and MKAR (Figure 16**Error! Reference source not found.**). These peaks are explained by body and seismic surface waves. In winter, microseisms exhibit similar trends with some difference as shown by Figure 11 c, Figure 12 c, Figure 13 c, Figure 14 c and Figure 16 b. The dominant directions are comparable with a larger spreading: from 250° to 360° and from 0° to 20°. For KKAR and MKAR, two peaks are seen in the histograms, with a second peak at 0-20°. These peaks could likely be explained by body and surface seismic phases identified by high trace velocity values. Microbaroms are predicted mainly from the southern direction (180-200°). Such a peak is observed only at IS31 and

Deleted: must …as beenbe…applied to account for wave coupli
Deleted: Figure 8Figure 7
Deleted: Figure 9Figure 8
Deleted: Figure 10Figure 9
Deleted: signal …ave attenuation for dominating sources locate
Formatted
Deleted: Figure 15
Formatted
Deleted: with
Formatted
Formatted
Deleted: Figure 15
Formatted
Deleted: Figure 8
Formatted
Deleted: Figure 9
Formatted
Deleted: Figure 10
Formatted
Deleted: Figure 15
Formatted
Formatted
Deleted: Figure 16
Formatted
Deleted: Figure 15
Formatted
Deleted: Figure 16
Formatted
Deleted: Figure 15
Formatted
Deleted: Figure 16
Formatted
Deleted: Figure 16
Formatted
Deleted: Figure 11
Formatted
Deleted: Figure 12
Formatted
Deleted: Figure 13
Formatted
Deleted: Figure 14
Formatted
Deleted: Figure 16
Formatted

MKAR (Figure 15 c). The closest peak observed at KURIS and MKIAR is shifted northwards by ~50°. The dominant back-azimuths are close to 90°. At MKIAR the peak is around 100°.

Thus, in winter, signals from ocean storms in the North Atlantic region dominate at all stations. This is supported by the microbarom and microseism simulation results which account for the predicted source regions, bathymetry, and propagation effects. More complicated picture is observed at summer months. Some stations detect signals from regions along the peri-Antarctic belt while simulations predict microbaroms with larger amplitude summer. Other stations detect signals from the south, but the detected back-azimuths disagree with the predictions.

Using historical IGR datasets, the spatiotemporal variability of microbarom signals due to changes in the source location and the structure of the atmospheric waveguides can be studied. There is a clear seasonal trend in the directions and amplitudes of microbaroms and microseisms (Figure 8, Figure 9 and Figure 10). Moreover, microseism amplitudes synchronously vary at all stations (Figure 17). A similar pattern is shown for microbaroms (Figure 18). A better agreement between observations and simulations is found for the azimuths.

As already shown by Evers and Siegmund (2009) and Smets and Evers (Smets and Evers, 2014), the life cycle of Sudden Stratospheric Warming (SSW) events can be inferred from the observed spatio-temporal variations of microbarom parameters. Such observations are noted at IS31 where microbaroms in early and late February 2017 shifted to easterly directions (~40°) consistent with the simulated source regions in the Northern Pacific (Figure 8). As noted for IS31, KURIS also recorded signals with back-azimuths of ~40° in late January 2017 (Figure 9). Similarly, signals from ~100° were also recorded during the 2017 SSW event at MKIAR. However, the observed back-azimuths differ from those expected (~60°). It is likely that this station recorded signals from other regions over the Pacific Ocean which are not described by the ocean wave model.
These findings are consistent with comparisons between the observed and modelled microbarom signals carried out by Landès et al. (2014) at IS31. This study shows that modelling well describes microbarom sources in the North Atlantic in winter and poorly explains signals in summer.

Comparison between seismic and infrasound bulletins at collocated sites highlight comment features. Figure 19 presents the observed back-azimuths and signal amplitudes from 1 January 2014 to 31 December 2017 at ABKAR and IS31 arrays located 230 km apart. Figure 20 shows the detections results for the collocated Kurchatov Cross and KURIS arrays. The comparison of the bulletins in Figure 19, and Figure 20 shows similar seasonal patterns:

- North Atlantic microseisms and microbaroms prevail in array records in winter months. Back-azimuths of approximately 300-360° are clearly visible in Figure 19 a,b, and Figure 20 a, b.
- Amplitudes of North Atlantic microbaroms and microseisms exceed large amplitude during summer months as shown by Figure 19 c,d, Figure 20 c,d.

At the same time, specific features are identified:

Deleted: Figure 15
Formatted
Formatted
Formatted
Deleted: .
Formatted
Deleted: However, during summer months, stations detect
Deleted: In this study, the method used to predict the attenuation
Deleted: Figure 7
Deleted: Figure 8
Deleted: Figure 9
Deleted: it is shown that the
Deleted: Figure 15Figure 11 and Figure 12
Deleted: Figure 18Figure 15
Deleted: The bathymetry effect plays an important role when
Formatted
Formatted
Deleted: Figure 7
Deleted: Figure 8
Deleted: , or inaccuracy in the used ECMWF products (Blanc et
Deleted: Landès et al., …014) at IS31. This study shows that
Deleted: of the
Deleted:
Deleted: for…t collocated the …ites where stations are collocat
Formatted
Deleted: Figure 19
Formatted
Deleted: record of…bserved back-azimuths and signal amplitud
Deleted: Figure 20
Formatted
Deleted: seismic array …nd KURIS infrasound station…rrays.
Formatted
Deleted: Figure 19
Deleted: Figure 20
Formatted
Deleted: series of …easonal patterns:. This comparison illustrat
Formatted
Deleted: Figure 19
Formatted
Deleted: and
Formatted
Deleted: Figure 20
Formatted
Deleted: and
Formatted
Deleted: significantly
Formatted
Formatted
Formatted
Formatted

- Arrays record North Atlantic microseisms more steadily than microbaroms from that region. Figure 19 a,b, Figure 20 b clearly show that microseisms dominate microbaroms.
- The range of back-azimuths for North Atlantic microseisms is larger than the ones of microbaroms for ABKAR and MKAR (Figure 19 a,b, and Figure 20 b).
- For all infrasound arrays, back-azimuths of North Atlantic microbaroms are larger (320-330°) (Figure 19 b and Figure 20 b). Back-azimuths differ from one seismic array to another: 330-350° for ABKAR array (Figure 19a), 290-310° for Kurchatov Cross array (Figure 20 a) and 310-320°.
- In summer months, no correlation is found in the prevailing directions of microseism and microbarom arrivals for collocated arrays (Figure 19 a and b, Figure 20 a,b)

This study provides a first characterization of the seasonal patterns of microbarom and microseisms recorded by the IGR seismo-acoustic network. The chosen detection algorithm and propagation model offer a good trade-off between low calculation effort and propagation accuracy. Identified shortcoming is the limitation of PMCC to detect overlapping microbarom sources originating from different directions. Furthermore, the approach assuming range-independent atmosphere may lead to erroneous interpretations for situations involving long propagation ranges where significant along-path variability of wind and temperature profiles may occur, in particular when modeling the relative strength of microbarom sources located in different hemispheres.

Conclusions

The IGR seismo-acoustic network is much denser than the global IMS infrasound network. Analyzing multi-year archives of continuous recordings provides a detailed picture of the spatial and temporal variability of the seismic and infrasound ambient noise originating from two hemispheres. In winter, the most intense oceanic storms are modelled in the Northern Atlantic and their signature prevails on infrasound and seismic records. During minor SSWs, bi-directional conditions may occur which may have strong impacts on the retrieved microbarom signals (Assink et al., 2014). Simulated and observed microbarom parameters are consistent, as shown by high correlation coefficients. The largest amplitudes of both microbaroms and microseisms are found for sources in the Northern Atlantic. Exploiting the synergy between seismic and infrasound ambient noise observations is thus valuable to: (i) better constrain the source strength using seismic records as microseisms propagation through the static structure of the Earth, (ii) improve the detectability of ocean-wave interaction and location accuracy as microbarom wave parameters are less affected by heterogeneities in the propagation medium, and (iii) improve the physical description of seismo-acoustic energy partitioning at the ocean-atmosphere interface.

Further numerical investigations are needed to define the most suitable detection parameters in terms of missed events and false alarm rate, and estimate wave parameter uncertainties accounting for the response functions of all arrays. In this study,

Deleted: Figure 19
Formatted ...
Deleted: and
Formatted ...
Deleted: Figure 20
Deleted: a and
Deleted: the quantity of recorded
Formatted ...
Deleted: exceeds …icrobaroms significantly ...
Formatted ...
Deleted: significantly more extensive
Formatted ...
Deleted: a visible range for the North Atlantic
Formatted ...
Deleted: R,
Formatted ...
Deleted: Figure 19
Formatted ...
Deleted: and
Formatted ...
Deleted: Figure 20
Deleted: a and
Formatted ...
Deleted: However, this distinction is not evident for a pair of ...
Formatted ...
Deleted: as shown by
Formatted ...
Deleted: Figure 19
Deleted: ,
Formatted ...
Formatted ...
Formatted ...
Formatted ...
Deleted: Figure 20
Formatted ...
Deleted: For all
Formatted ...
Deleted: s, back-azimuths differ not only from each other, bu ...
Formatted ...
Deleted: The range of back-azimuths is about
Formatted ...
Deleted: Figure 19
Formatted ...
Deleted: ;
Formatted ...
Formatted ...
Formatted ...
...
Formatted ...
Formatted ...
Formatted ...

part of the discrepancies between observations and predictions motivate the use of high-resolution detection methods to identify multiple propagation paths from which microbarom energy can reach the array (e.g., Assink et al., 2014). Exploring the capability of high-resolution detection processing techniques to extract multidirectional overlapping coherent energy would be valuable to provide a more realistic picture of the recorded ocean ambient noise (e.g., den Ouden et al., 2020).

Additional studies are required to further evaluate whether the bathymetry effect could explain discrepancies between the observed microbarom and microseism signals (Longuet-Higgins, 1950; Stutzmann et al., 2012, De Carlo 2020). In summer, the microbarom and microseism sources which dominate in the southern hemisphere more especially along the peri-antarctic belt are likely at the origin of the weak signals observed south of the IGR network. For such long propagation ranges, more realistic numerical simulations could reduce the differences between the observed and modelled amplitude; additional studies are thus required to explore time- and range-dependent full-wave propagation techniques while still maintaining computational efficiency (e.g., Waxler and Assink, 2019). Including additional data from other seismo-acoustic network in the southern hemisphere would help validating long-range propagation modelling, better characterize station-specific ambient noise signatures, and enhance discrimination methods at a regional scale.

Deleted: using range dependent atmosphere models

Deleted: .

Code/Data availability

Atmospheric wind and temperature profiles are derived from operational high-resolution atmospheric model analysis, defined by the Integrated Forecast System of the ECMWF, available at https://www.ecmwf.int/ (last access: 2 September 2019; ECMWF, 2018). Waveform data for the seismic and infrasound arrays of the CTBTO IMS (https://www.ctbto.org/, last access: 2 September 2019) used in this study are available to the authors, being members of National Data Centers for the CTBTO. Data of the Kazakhstani national seismic and infrasound arrays are available under request from the Institute of Geophysical Researches, National Nuclear Center of Kazakhstan. Results of the microseism and microbarom detections by the seismo-acoustic Kazakh network and of the microbarom simulation for the infrasound arrays of the network are available at ISC repository (Smirnov et al., 2020).

Author contribution

N. Shapiro and A. Le Pichon suggested main outlines of the paper. A. Smirnov and A. Le Pichon prepared historical dataset for processing. M. De Carlo and A. Le Pichon developed the microbarom source model. A. Smirnov performed microbarom and microseism detections and propagation simulations. A. Smirnov prepared the manuscript with contributions from all co-authors. A. Le Pichon, M. De Carlo and S. Kulichkov made critical reviews and comments to improve the manuscript.

Competing interests

The authors declare that they have no conflict of interest.

Acknowledgements

This research has been supported by the Commissariat à l'Energie Atomique (CEA, France). The work of NS has been supported by the European Research Council (ERC) under the European Union Horizon 2020 Research and Innovation Programme (grant agreement 787399-SEISMAZE), the Russian Ministry of Education and Science (grant N 14.W03.31.0033)

Deleted: a`

and Russian Foundation for Basic Research (project no. 18-05-00576). Authors also thank Anna Smirnova for the help in the manuscript preparation.

References

Ardhuin, F., Stutzmann, E., Schimmel, M. and Mangeney, A.: Ocean wave sources of seismic noise, J. Geophys. Res., 116(C9), doi:10.1029/2011jc006952, 2011.

Ardhuin, F. and Herbers, T. H. C.: Noise generation in the solid Earth, oceans and atmosphere, from nonlinear interacting surface gravity waves in finite depth, J. Fluid Mech., 716, 316–348, doi:10.1017/jfm.2012.548, 2013a.

Ardhuin, F., Lavanant, T., Obrebski, M.: A numerical model for ocean ultra-low frequency noise: wave-generated acoustic-gravity and Rayleigh modes, J. Acoust. Soc. Am., 134, doi:10.1121/1.4818840, 2013b.

Assink, J. D., Waxler, R., Smets, P. and Evers, L. G.: Bidirectional infrasonic ducts associated with sudden stratospheric warming events, J. Geophys. Res. Atmos., 119(3), 1140–1153, doi:10.1002/2013jd021062, 2014.

Belyashov, A., Dontsov, V., Dubrovin, V., Kunakov, V. and Smirnov, A.: New infrasound array “Kurchatov”, NNC RK Bull., (2), 24–30, 2013.

Cansi, Y.: An automatic seismic event processing for detection and location: The P.M.C.C. Method, Geophys. Res. Lett., 22(9), 1021–1024, doi:10.1029/95gl00468, 1995.

Cansi, Y. and Klinger, Y.: An Automated Data Processing Method for Mini-Arrays, Newsl. Eur. Seismol. Cent., 1021–1024, 1997.

Capon, J.: Long-Period Signal Processing Results for LASA, NORSAR and ALPA, Geophys. J. Int., 31(1–3), 279–296, doi:10.1111/j.1365-246x.1972.tb02370.x, 1972.

De Carlo, M., Le Pichon, A., Ardhuin, F. and Näsholm, S.: Characterizing and modelling ocean ambient noise using infrasound network and middle atmospheric models, NNC RK Bull., (2), 144–151, 2018.

De Carlo, M., Ardhuin, F., and Le Pichon, A.: Atmospheric infrasound generation by ocean waves in finite depth: unified theory and application to radiation patterns, Geophys. J. Int., 21, 569-585, doi:10.1093/gji/ggaa015, 2020.

Donn, W. L., and Naini, B.: Sea wave origin of microbaroms and microseisms, J. Geophys. Res., 78, 4482-4488, doi:10.1029/JC078i021p04482, 1973.

Ceranna, L., Matoza, R., Hupe, P., Le Pichon, A. and Landès, M.: Systematic array processing of a decade of global IMS infrasound data, Infrasound monitoring for atmospheric studies, 2nd ed. Springer Nature, Dordrecht, ISBN: 978-3-319-75140-5, 471–482, 2019.

Evers, L. G. and Haak, H. W.: Listening to sounds from an exploding meteor and oceanic waves, Geophys. Res. Lett., 28(1), 41–44, doi:10.1029/2000gl011859, 2001.

Evers, L. G. and Siegmund, P.: Infrasonic signature of the 2009 major sudden stratospheric warming, Geophys. Res. Lett., 36(23), doi:10.1029/2009gl041323, 2009.

Garcés, M.: On using ocean swells for continuous infrasonic measurements of winds and temperature in the lower, middle, and upper atmosphere, Geophys. Res. Lett., 31(19), doi:10.1029/2004gl020696, 2004.

Gutenberg, B.: Microseisms, microbaroms, storms, and waves in western North America, Eos Trans. AGU, 34(2), 161-173, doi:10.1029/TR034i002p00161, 1953.

Hasselmann, K.: A statistical analysis of the generation of microseisms, Rev. Geophys., 1(2), 177, doi:10.1029/rg001i002p00177, 1963.

Hasselmann, K.: Feynman diagrams and interaction rules of wave-wave scattering processes, Rev. Geophys., 4(1), 1, doi:10.1029/rg004i001p00001, 1966.

Haubrich, R. A. and McCamy, K.: Microseisms: Coastal and pelagic sources, Rev. Geophys., 7(3), 539, doi:10.1029/rg007i003p00539, 1969.

Hupe, P., Ceranna, L., Pilger, C., De Carlo, M., Le Pichon, A., Kaifler, B. and Rapp, M.: Assessing middle atmosphere weather models using infrasound detections from microbaroms, Geophys. J. Int., 216(3), 1761–1767, doi:10.1093/gji/ggy520, 2018.

IFREMER: Wave Watch 3, [online] Available from: ftp://ftp.ifremer.fr/ifremer/ww3/ (Accessed 3 October 2018), 2018.

Kanamori, H. and Given, J. W.: Use of long-period surface waves for rapid determination of earthquake-source parameters, Phys. Earth Planet. Inter., 27(1), 8–31, doi:10.1016/0031-9201(81)90083-2, 1981.

Kedar, S., Longuet-Higgins, M., Webb, F., Graham, N., Clayton, R. and Jones, C.: The origin of deep ocean microseisms in the North Atlantic Ocean, Proc. R. Soc. A Math. Phys. Eng. Sci., 464(2091), 777–793, doi:10.1098/rspa.2007.0277, 2008.

KNDC: Observation network of the Institute of Geophysical Researches of the National Nuclear Center of the Republic of Kazakhstan., [online] Available from: http://www.kndc.kz/index.php?option=com_content&view=article&id=45&Itemid=147&lang=en (Accessed 3 October 2019), 2019.

Landès, M., Ceranna, L., Le Pichon, A. and Matoza, R. S.: Localization of microbarom sources using the IMS infrasound network, J. Geophys. Res. Atmos., 117(D6), n/a-n/a, doi:10.1029/2011jd016684, 2012.

Landès, M., Le Pichon, A., Shapiro, N. M., Hillers, G. and Campillo, M.: Explaining global patterns of microbarom observations with wave action models, Geophys. J. Int., 199(3), 1328–1337, doi:10.1093/gji/ggu324, 2014.

Longuet-Higgins, M. S.: A Theory of the origin of microseisms, Philos. Trans. R. Soc. A Math. Phys. Eng. Sci., 243(857), 1–35, doi:10.1098/rsta.1950.0012, 1950.

Matoza, R. S., Landès, M., Le Pichon, A., Ceranna, L. and Brown, D.: Coherent ambient infrasound recorded by the International Monitoring System, Geophys. Res. Lett., 40(2), 429–433, doi:10.1029/2012gl054329, 2013.

Olson, J. V and Szuberla, C. A. L.: Distribution of wave packet sizes in microbarom wave trains observed in Alaska, J. Acoust. Soc. Am., 117(3), 1032–1037, doi:10.1121/1.1854651, 2005.

Le Pichon, A., Ceranna, L. and Vergoz, J.: Incorporating numerical modeling into estimates of the detection capability of the IMS infrasound network, J. Geophys. Res. Atmos., 117(D5), n/a-n/a, doi:10.1029/2011jd016670, 2012.

Le Pichon, A., Assink, J. D., Heinrich, P., Blanc, E., Charlton-Perez, A., Lee, C. F., Keckhut, P., Hauchecorne, A., Rüfenacht, R., Kämpfer, N., Drob, D. P., Smets, P. S. M., Evers, L. G., Ceranna, L., Pilger, C., Ross, O. and Claud, C.: Comparison of co-located independent ground-based middle atmospheric wind and temperature measurements with numerical weather prediction models, J. Geophys. Res. Atmos., 120(16), 8318–8331, doi:10.1002/2015jd023273, 2015.Obrebski, M., F. Ardhuin,

Field Code Changed

Deleted: Hagerty, M. T., Kim, W.-Y. and Martysevich, P.: Infrasound Detection of Large Mining Blasts in Kazakstan, Pure Appl. Geophys., 159(5), 1063–1079, doi:10.1007/s00024-002-8673-3, 2002.¶

Deleted: d

Deleted: Liszka, L. and Waldemark, K.: High Resolution Observations of Infrasound Generated by the Supersonic Flights of Concorde, J. Low Freq. Noise, Vib. Act. Control, 14(4), 181–192, doi:10.1177/026309239501400403, 1995.¶

Deleted: O

Deleted: M

Formatted: List Paragraph, Widow/Orphan control, Adjust space between Latin and Asian text, Adjust space between Asian text and numbers

Deleted: ¶

F., E. Stutzmann, E., and M. Schimmel, M.: Detection of microseismic compressional (P)body waves aided by numerical modeling of oceanic noise sources,J. Geophys. Res. Solid Earth, 118, 4312–4324, doi:10.1002/jgrb.50233, 2013.

den Ouden, O., Assink, J. D., Smets, P., Shani-Kadmiel, S., Averbuch, G., and Evers, L.: CLEAN beamforming for the enhanced detection of multiple infrasonic sources, Geophys. J. Int, 221 (1), 305-317, doi:10.1093/gji/ggaa010, 2020.

Shapiro, N. M.: High-Resolution Surface-Wave Tomography from Ambient Seismic Noise, Science (80-.)., 307(5715), 1615–1618, doi:10.1126/science.1108339, 2005.

Shapiro, N. M. and Campillo, M.: Emergence of broadband Rayleigh waves from correlations of the ambient seismic noise, Geophys. Res. Lett., 31(7), doi:10.1029/2004gl019491, 2004.

Smets, P. S. M. and Evers, L. G.: The life cycle of a sudden stratospheric warming from infrasonic ambient noise observations, J. Geophys. Res. Atmos., 119(21), 12-84,99, doi:10.1002/2014jd021905, 2014.

Smirnov, A.: The variety Oof Infrasound sources recorded by Kazakhstani stations, in CTBT: Science and Technology, Vienna. [online] Available from: https://www.ctbto.org/fileadmin/user_upload/SnT2015/SnT2015_Posters/T2.3-P20.pdf, 2015.

Smirnov, A., Dubrovin, V., Evers, L. G. and Gibbons, S. J.: Explanation of the nature of coherent low-frequency signal sources recorded by the monitoring station network of the NNC RK, in CTBT: Science and Technology 2011. [online] Available from: https://www.ctbto.org/fileadmin/user_upload/SandT_2011/posters/T4-P12 A_Smirnov Explanation of the nature of coherent low-frequency signal sources recorded by the monitoring station.pdf, 2011.

Smirnov, A., De Carlo, M., Le Pichon, A. and Shapiro, N. M.: Signals from severe ocean storms in North Atlantic as it detected in Kazakhstan: observations and modelling, NNC RK Bull., (2), 152–160, 2018.

Smirnov, A., De Carlo, M., Le Pichon, A., Shapiro, N. and Kulichkov, S.: Results of the microseism and microbarom detections by the seismo-acoustic Kazakh network, doi:10.31905/dsw7l5bv, 2020.

Stehly, L., Campillo, M. and Shapiro, N. M.: A study of the seismic noise from its long-range correlation properties, J. Geophys. Res., 111(B10), doi:10.1029/2005jb004237, 2006.

Stutzmann, E., Ardhuin, F., Schimmel, M., Mangeney, A. and Patau, G.: Modelling long-term seismic noise in various environments, Geophys. J. Int., 191(2), 707–722, doi:10.1111/j.1365-246x.2012.05638.x, 2012.

Szuberla, C. A. L. and Olson, J. V: Uncertainties associated with parameter estimation in atmospheric infrasound arrays, J. Acoust. Soc. Am., 115(1), 253–258, doi:10.1121/1.1635407, 2004.

Toksöz MN, Lacoss RT. Microseisms: mode structure and sources. Science. 1968; 159 (3817): 872-873. doi:10.1126/science.159.3817.872

Waxler, R. and Gilbert, K. E.: The radiation of atmospheric microbaroms by ocean waves, J. Acoust. Soc. Am., 119(5), 2651–2664, doi:10.1121/1.2191607, 2006.

Waxler, R., Gilbert, K., Talmadge, C., and Hetzer, C.: The effects of finite depth of the ocean on microbarom signals, in 8th Int. Conf. Theoretical and Computational Acoustics (ICTCA), Crete, Greece, 2007.

Waxler, R., and Assink, J.: Propagation modeling through realistic atmosphere and benchmarking. In Infrasound monitoring

Formatted: Check spelling and grammar
Deleted: n/a-n/a,
Deleted: 12,
Deleted: V
Deleted: S
Deleted: R
Deleted: B
Deleted: K
Deleted: S
Deleted: d
Formatted: Highlight
Commented [ALP3]: Rewrite reference, no abreviation
Deleted: and of the microbarom simulation for the infrasound arrays of the network
Deleted: Results microseism microbarom Detect. by Seism. Kazakh Netw. microbarom Simul. infrasound arrays Netw.,
Deleted: ToksoZ, M. N. and Lacoss, R. T.: Microseisms: mMode sStructure and sSources, Science (80-.???)., 159(3817), 872–873, doi:10.1126/science.159.3817.872, 1968.
Formatted: Superscript
Formatted: Left

for atmospheric studies: 2nd ed. Springer Nature, Dordrecht, ISBN: 978-3-319-75140-5, 509-550, 2019.

Weaver, R. L.: GEOPHYSICS: Information from Seismic Noise, Science 80, 307(5715), 1568–1569, doi:10.1126/science.1109834, 2005.

1165

Formatted: Superscript

Deleted: (

Deleted: -.).

Commented [ALP5]: Check reference

Deleted: Wilson, C. R.: Auroral infrasonic waves and poleward expansions of auroral substorms at Inuvik, N.W.T., Canada, Geophys. J. R. astr. Soc., 26, 179–181, 1971.¶

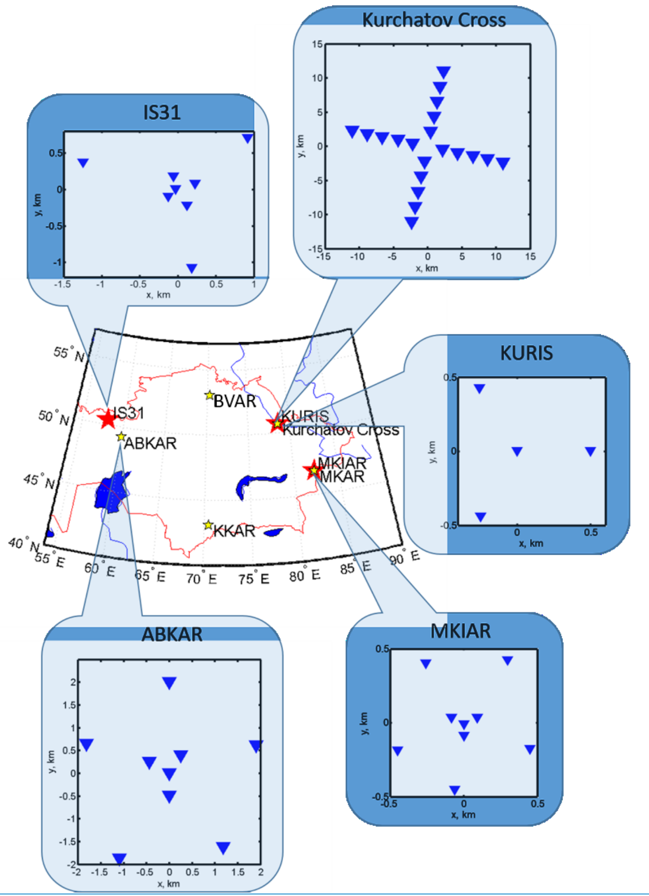

Figure 1. IGR monitoring network. Yellow and red stars are seismic and infrasound arrays, respectively. Seismic and infrasound arrays are collocated at two sites. IS31 infrasound and ABKAR seismic arrays are located 200 km apart. Callouts show the array configurations. the configurations are not shown for the KKAR and MKAR as they are similar to the ABKAR's one.

Formatted: English (United States)

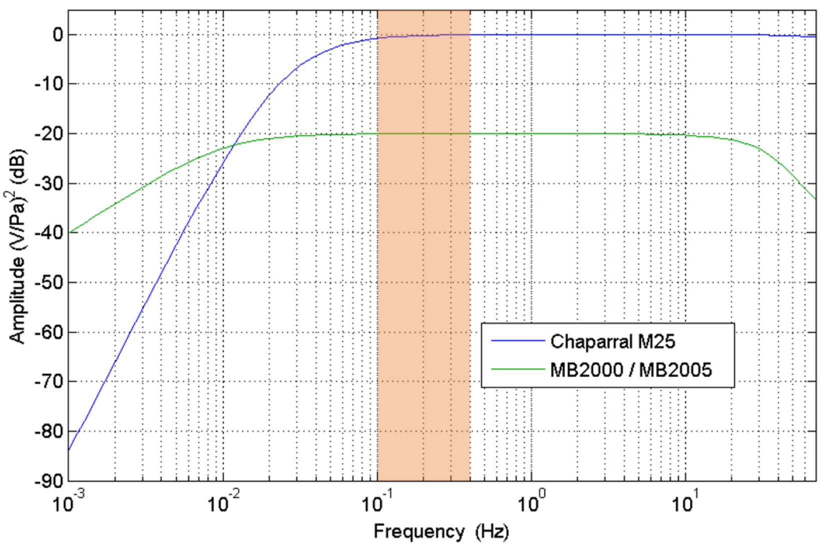

Figure 2. **Frequency response of the MB2000, MB2005 and Chaparral M25 microbarometers.**

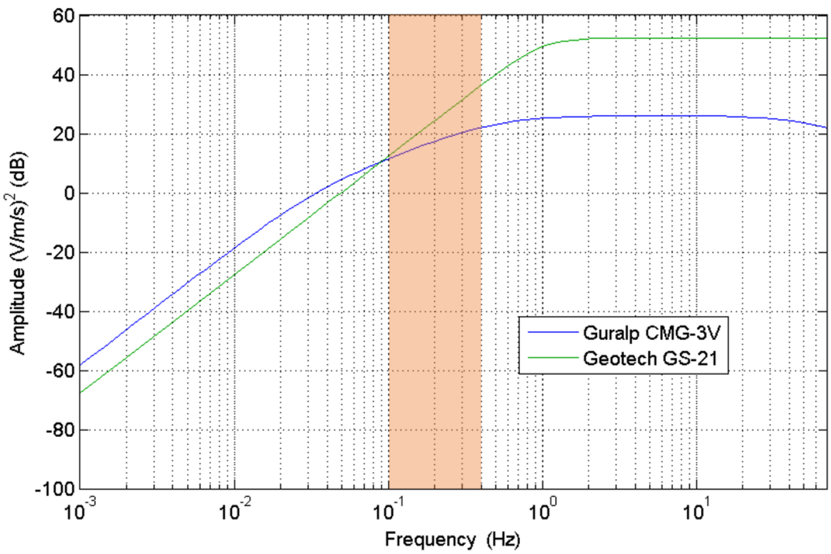

Figure 3. Frequency responses of Geotech GS-21 Guralp CMG-3V seismometers

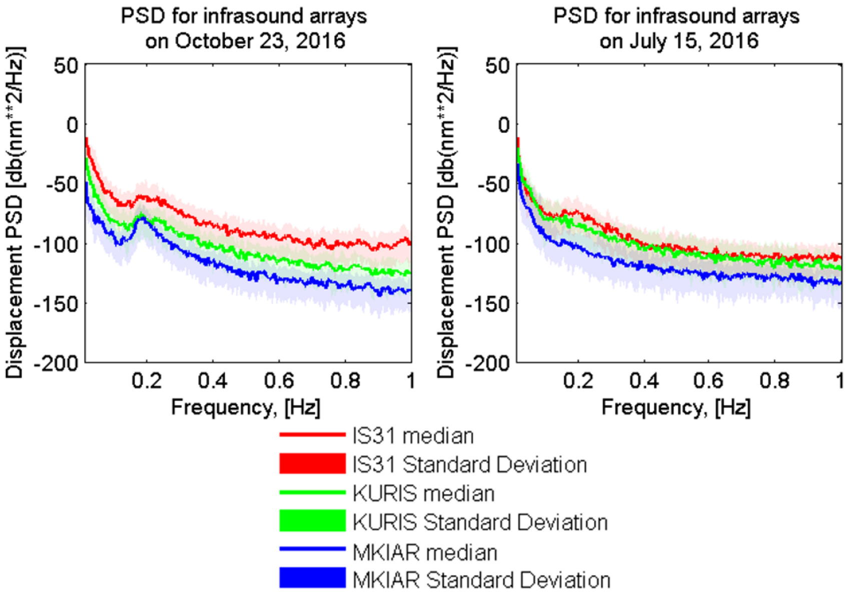

1185

Figure 4. **Noise spectra characteristics for the infrasound arrays.**

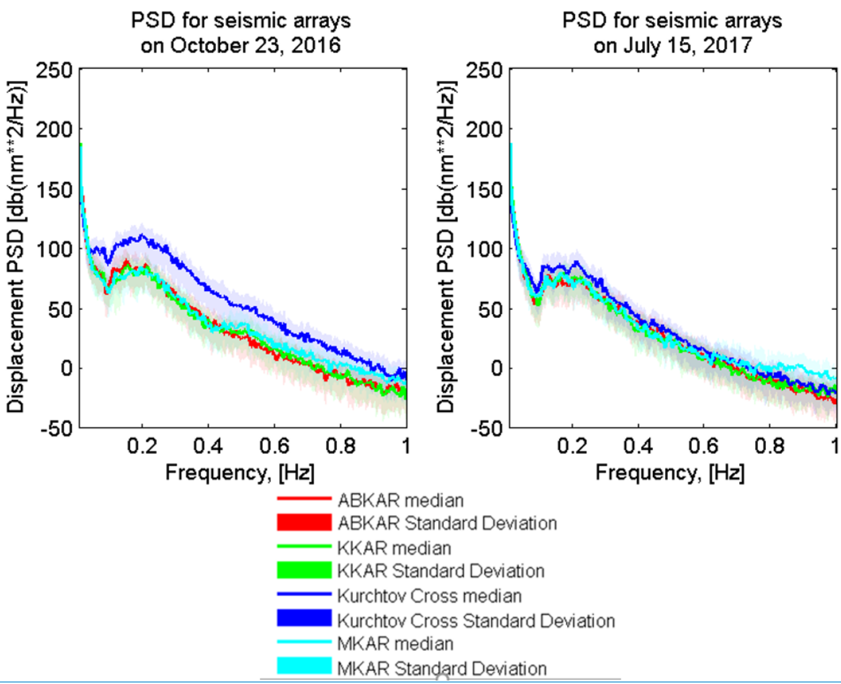

Figure 5. Noise spectra characteristics for the seismic arrays.

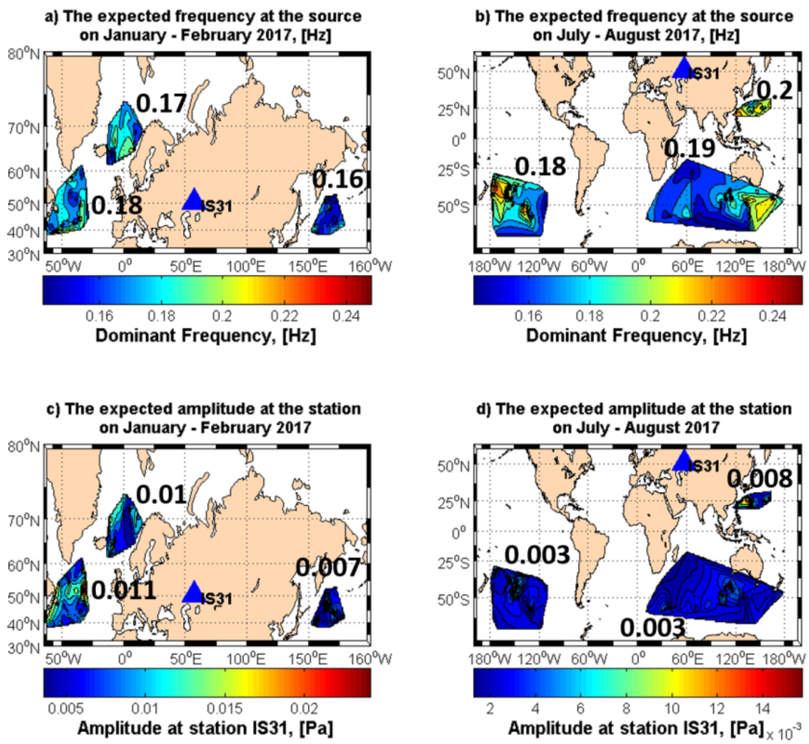

Figure 6. The distribution of the epicenters of the expected microbarom sources in January - February 2017 detected by the IS31 infrasound array.

Deleted: for the

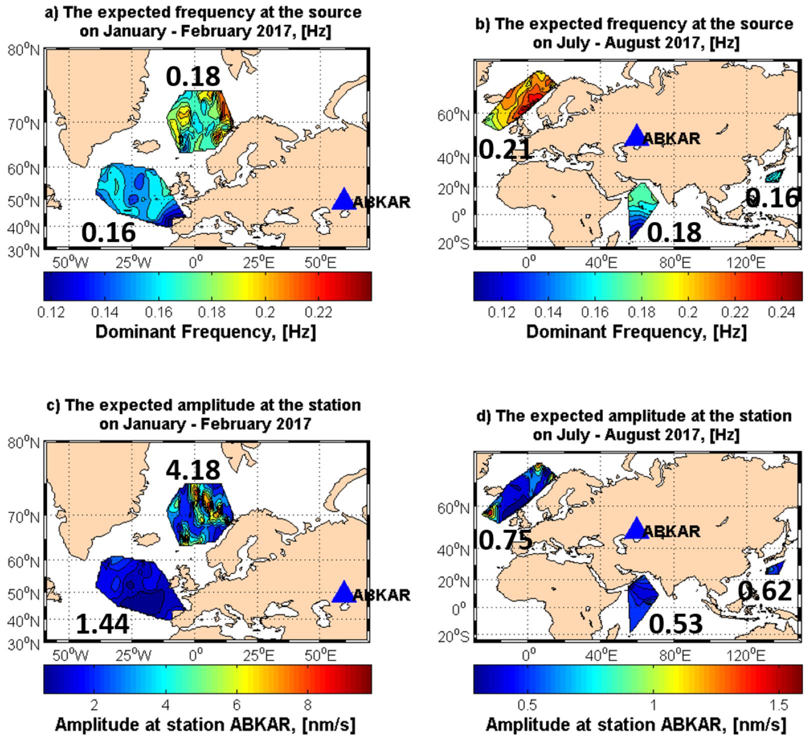

Figure 7. The distribution of the epicenters of the predicted microseism sources from January to February 2017 detected by the ABKAR seismic array.

Deleted: expected

Deleted: in

Deleted: -

Deleted: for the

Deleted: at

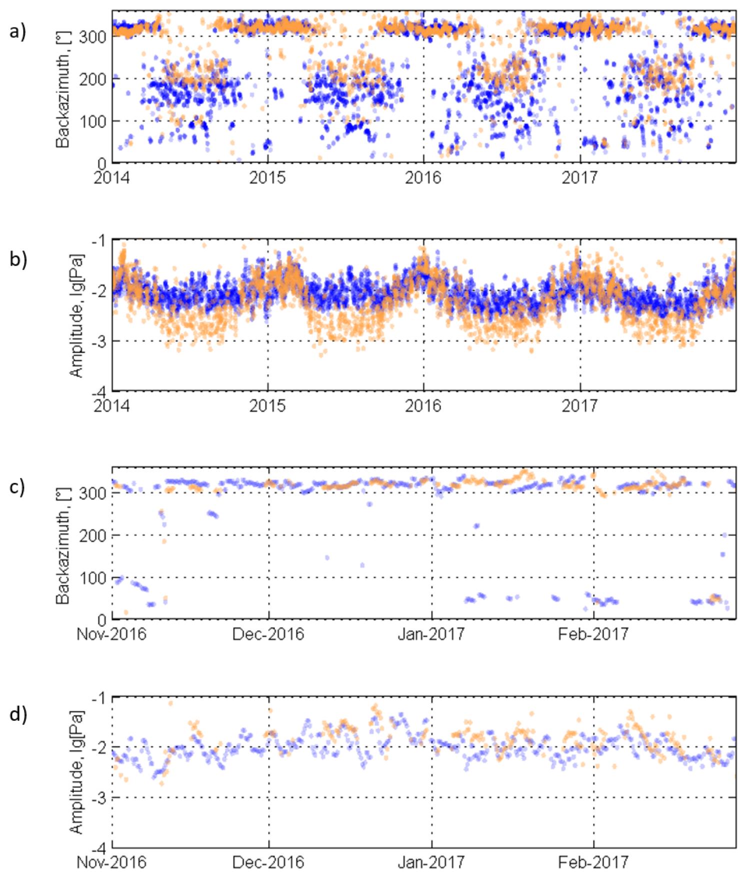

Figure 8. Dominant amplitude and back-azimuths of infrasound signals at IS31 with a time resolution of 6 hours from 1 January 1, 2014 to December 31, 2017 (orange circles). Blue circles denote simulated values. (c) and (d): detail from November 1, 2016 to February 28, 2017.

Deleted:

Deleted: ,

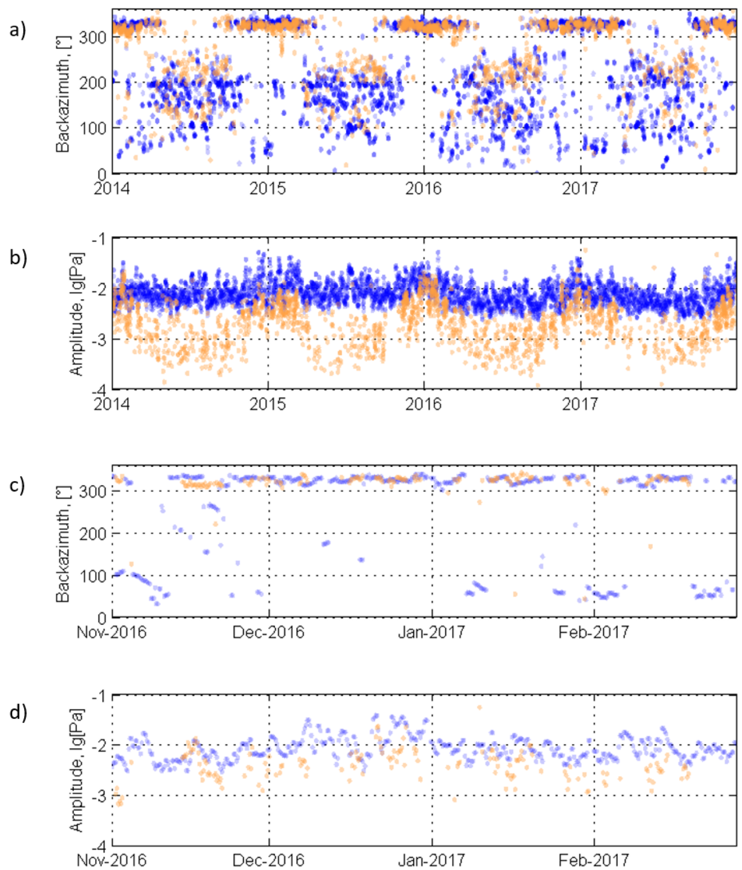

Figure 9. Same as Figure 8 at KURIS every from 1 January 1, 2014 to December 31, 2017.

Deleted: for

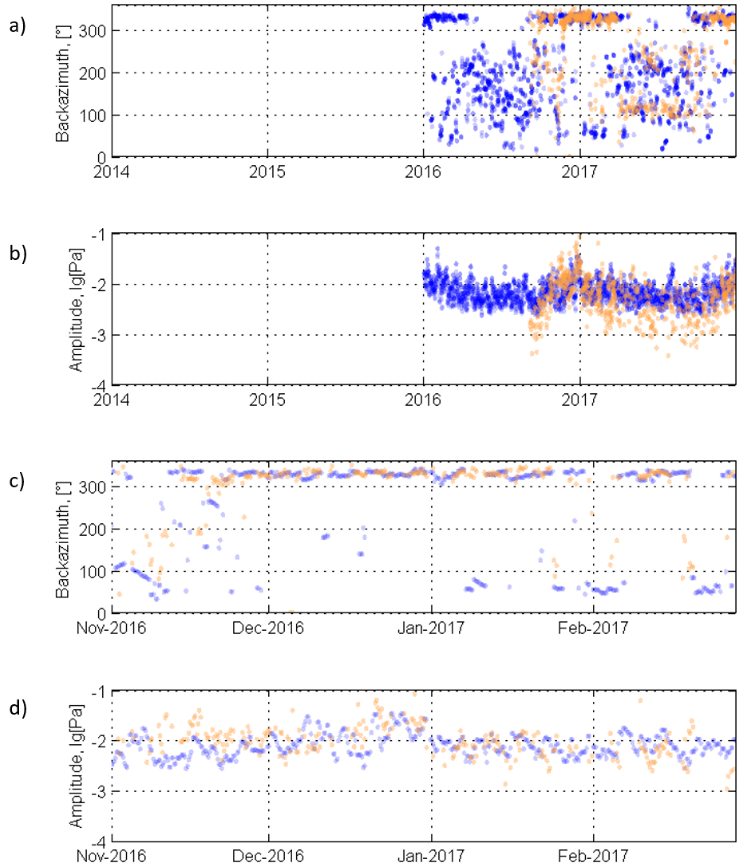

1220 Figure 10. Same as Figure 8 at MKIAR from 1 January 1, 2014 to December 31, 2017.

Deleted: for

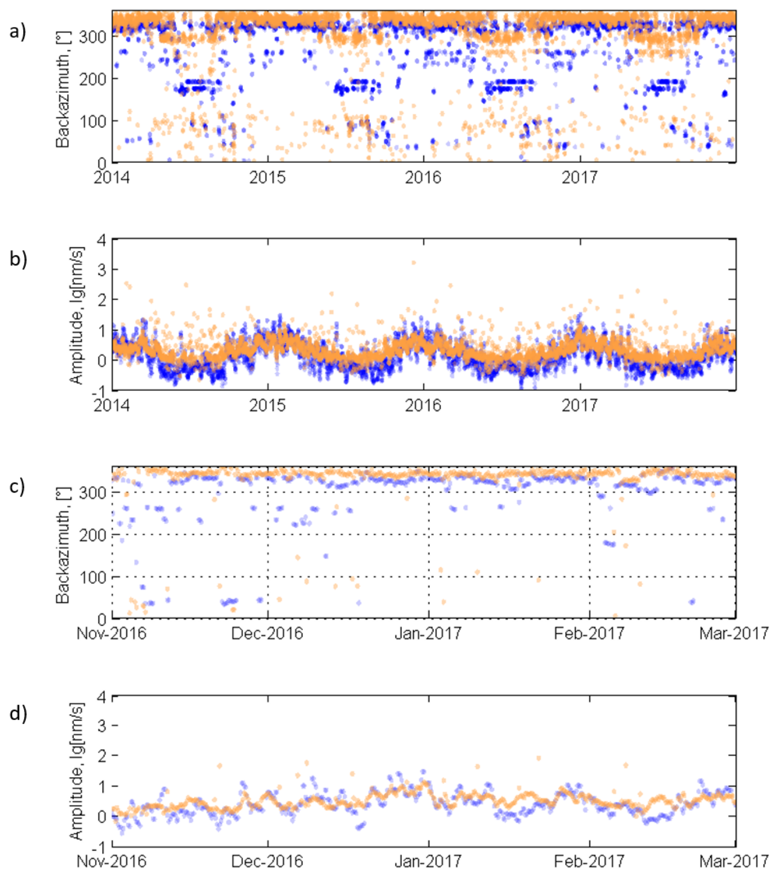

Figure 11. Same as Figure 8 at ABKAR from 1 January 1, 2014 to December 31, 2017.

Deleted: for

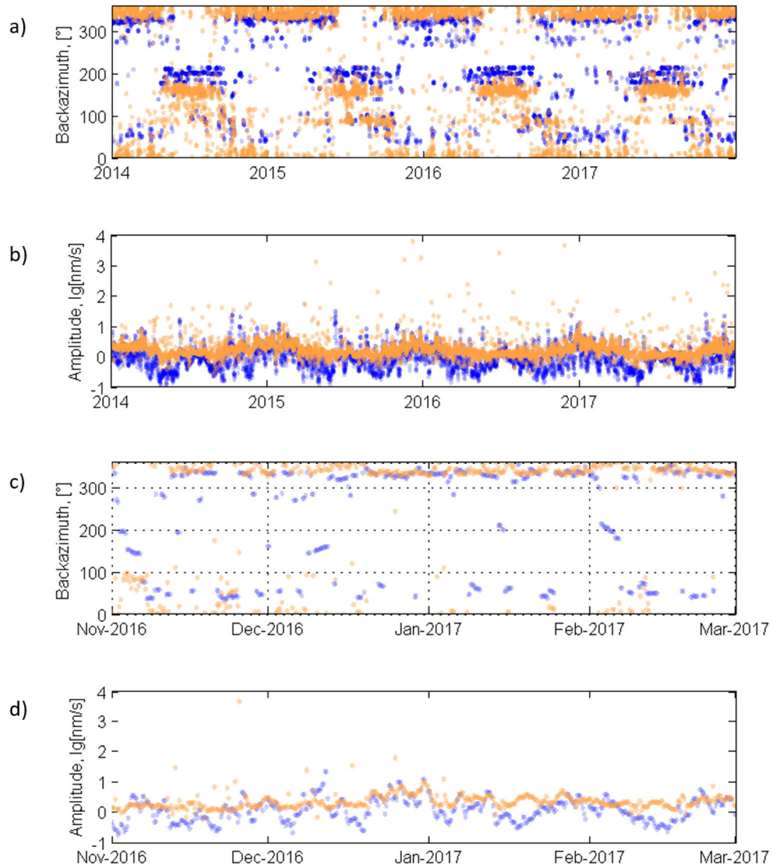

Figure 12. Same as Figure 8 at KKAR from 1 January 1, 2014 to December 31, 2017.

Deleted: for

1230

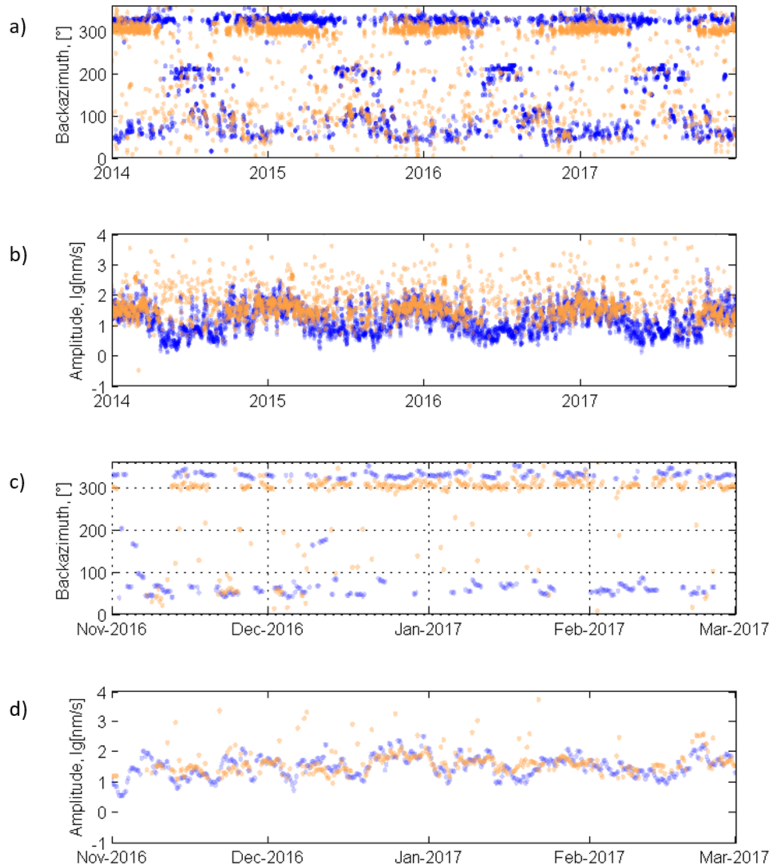

Figure 13. Same as Figure 8 at Kurchatov Cross from 1 January 1, 2014 to December 31, 2017. Expected amplitudes are scaled to compensate the instrument response difference.

Deleted: for

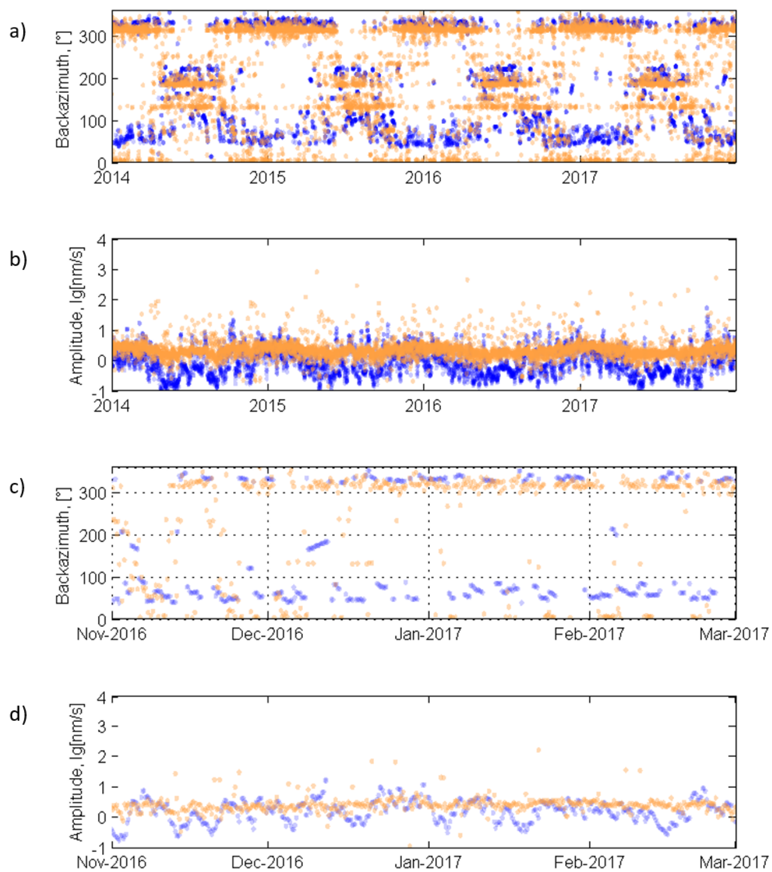

1235 **Figure 14.** Same as Figure 8 at MKAR from 1 January 1, 2014 to December 31, 2017.

Deleted: for

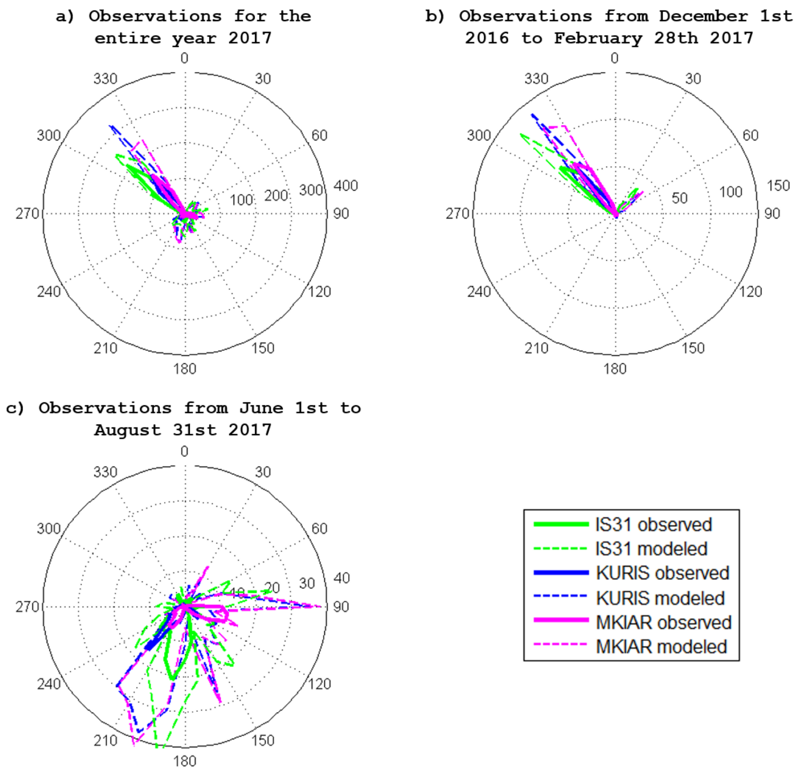

Figure 15. Azimuthal distribution of detections with maximum amplitudes for infrasound stations throughout 2017 (a), from December 1, 2016, to February 28, 2017 (b), and from June 1 to August 31, 2017 (c).

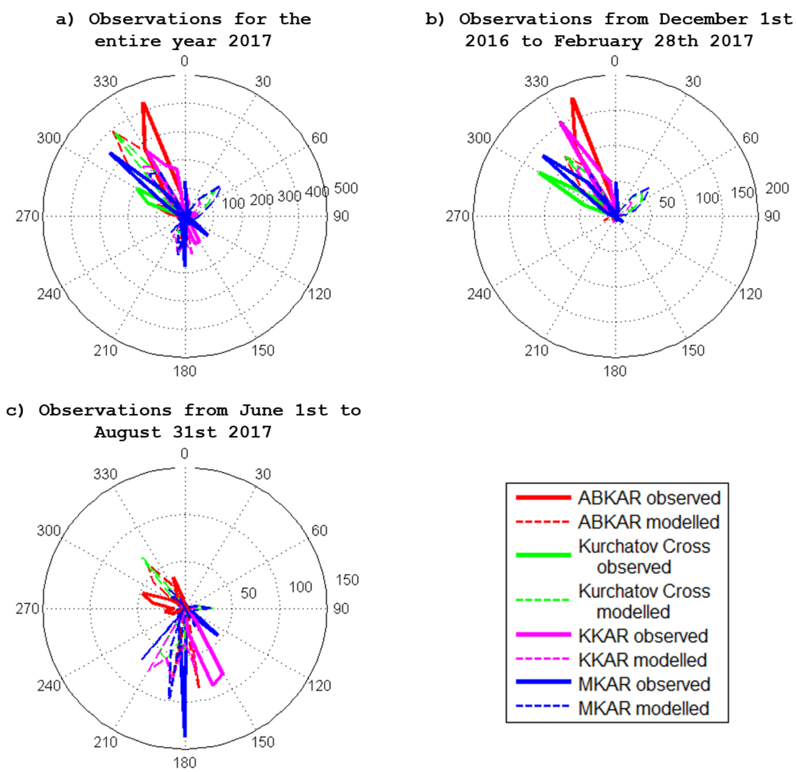

Figure 16. Azimuthal distribution of detections with maximum amplitudes for seismic stations throughout 2017 (a), from December 1, 2016, to February 28 (b), 2017, and from June 1 to August 31, 2017 (c).

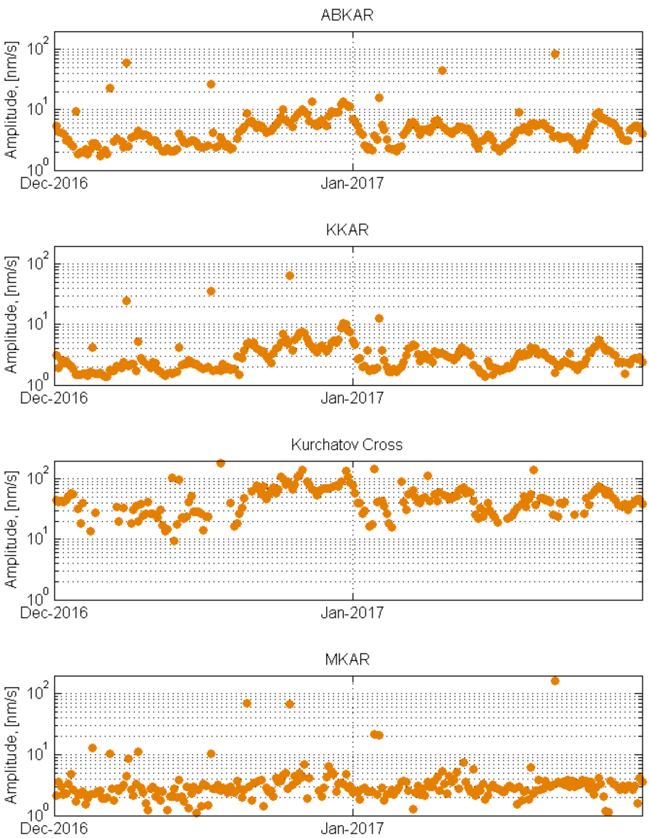

Figure 17. Dominant amplitude of seismic signals in the 0.1-0.4 Hz band detected at ABKAR (a), KKAR (b), Kurchatov Cross array (c), and MKAR (d) arrays from December 1, 2016 to January 31, 2017.

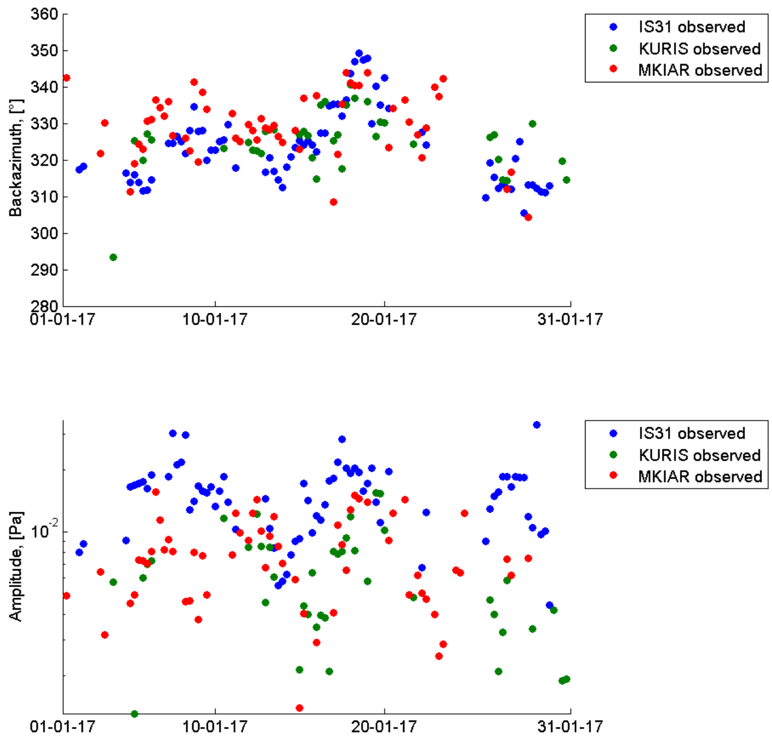

Figure 18. **Spatio-temporal variations of microbarom parameters recorded at IS31, KURIS, and MKIAR. Back-azimuth (top) and amplitude (bottom) variations during January 2017.**

Deleted: A

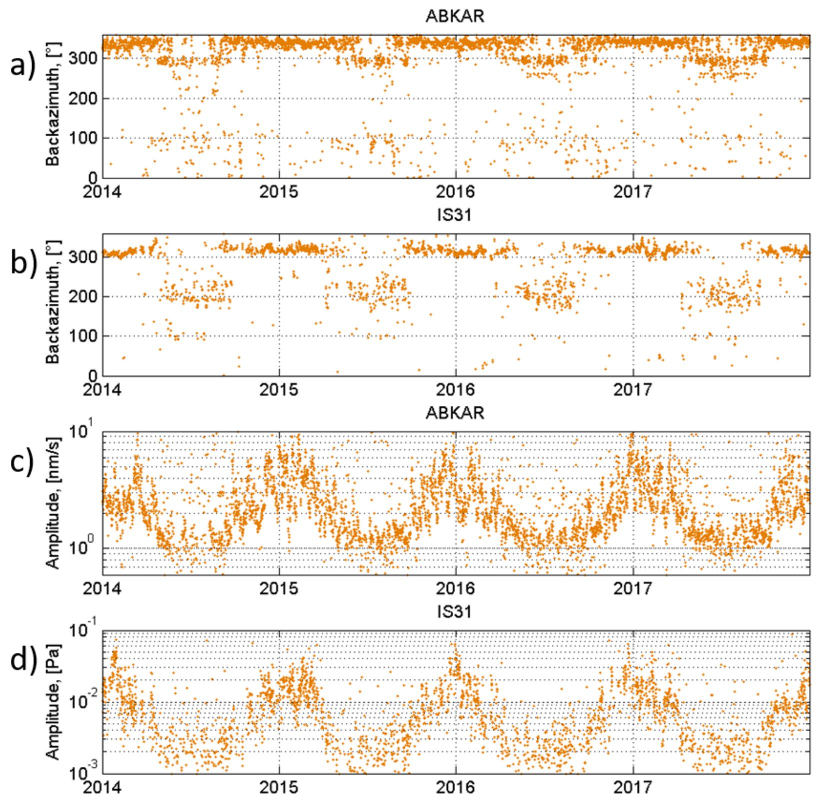

Figure 19. **Comparison of the observation results at the ABKAR seismic array and IS31 infrasound station separated by 230 km.**

Deleted: closely placed

Deleted: . The distance between stations is

Formatted: English (United States)

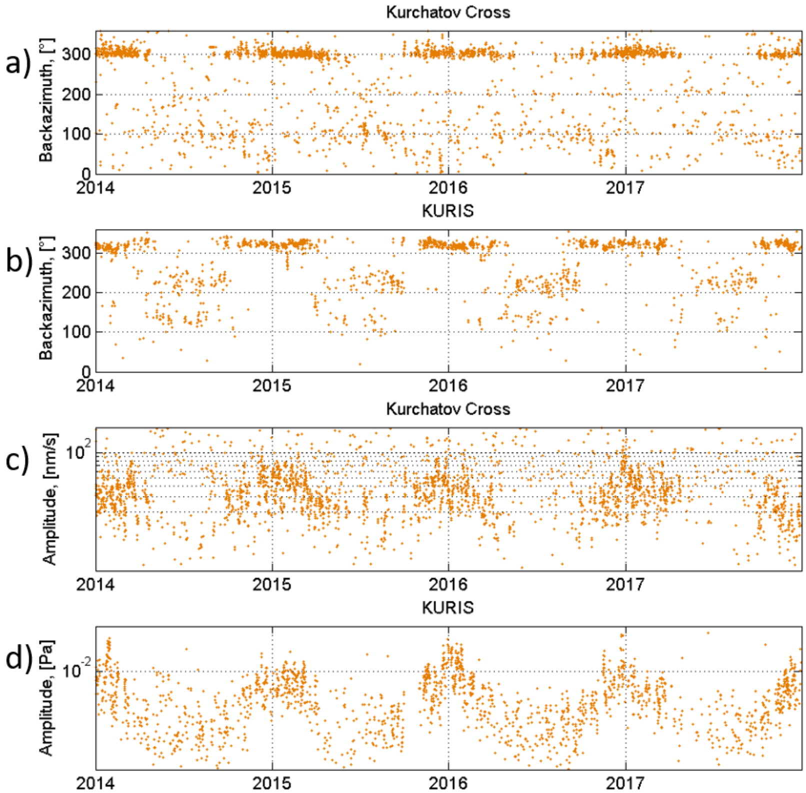

Figure 20. Comparison of the observation results at the collocated Kurchatov Cross seismic array and KURIS infrasound station.

Table 1. Uncertainties of azimuth and apparent velocity estimates.

Parameter	Horizontal velocity, m/s	IS31	KURIS	MKIAR	ABKAR	KKAR	MKAR	Kurchatov Cross

δΘ (°)	340	0.55 - 0.74	2.05 – 2.34	0.58 - 0.67	-	-	-	-
δV (m/s)		3.8 – 4.4	12 - 14	3.5 – 3.9	-	-	-	-
δΘ (°)	3000	-	-	-	4.89 – 5.64	5.14 – 6.30	4.55 – 6.84	0.48 – 0.49
δV (m/s)		-	-	-	250 – 290	270 – 330	220 - 380	25 – 26

Table 2. Estimations of the prediction quality for microbarom amplitudes and azimuths.

Station	Long-term Observation period	S_{corr_Az}	S_{corr_Amp}	Observation period on winter	S_{corr_Az}	S_{corr_Amp}	Observation period on summer	S_{corr_Az}	S_{corr_Amp}
IS31	2014 - 2017	0.61	0.39	Dec 2016 – Feb 2017	0.76	0.53	Jun 2017 – Aug 2017	0.44	0.26
KURIS	2014 - 2017	0.52	0.23	Dec 2016 – Feb 2017	0.82	0.58	Jun 2017 – Aug 2017	0.16	0.18
MKIAR	Sep 2016 – Dec 2017	0.62	0.5	Dec 2016 – Feb 2017	0.82	0.66	Jun 2017 – Aug 2017	0.34	0.39

Deleted: ,

Deleted: ¶
¶
¶